Direct numerical simulation of a passive scalar with imposed mean gradient in isotropic turbulence

M. R. Overholt[a] and S. B. Pope
Sibley School of Mechanical and Aerospace Engineering, Cornell University, Ithaca, New York 14853

(Received 20 March 1996; accepted 30 July 1996)

Mixing of a passive scalar in statistically homogeneous, isotropic, and stationary turbulence with a mean scalar gradient is investigated via direct numerical simulation, for Taylor-scale Reynolds numbers, R_λ, from 28 to 185. Multiple independent simulations are performed to get confidence intervals, and local regression smoothing is used to further reduce statistical fluctuations. The scalar fluctuation field, $\phi(\mathbf{x},t)$, is initially zero, and develops to a statistically stationary state after about four eddy turnover times. Quantities investigated include the dissipation of scalar flux, which is found to be significant; probability density functions (pdfs) and joint-pdfs of the scalar, its derivatives, scalar dissipation, and mechanical dissipation; and conditional expectations of scalar mixing, $\nabla^2\phi$. A linear model for scalar mixing jointly conditioned on the scalar and v-velocity is developed, and reproduces the data quite well. Also considered is scalar mixing jointly conditioned on the scalar and scalar dissipation. Terms appearing in the balance equation for the pdf of ϕ are examined. From a solution of the scalar pdf equation two sufficient conditions arise for the scalar pdf to be Gaussian. These are shown to be well satisfied for moderate values of the scalar, and approximately so for large fluctuations. Many correlations are also presented, including $\rho(v,\phi)$, which changes during the evolution of the scalar from a value of unity when initialized to the stationary value of 0.5–0.6. [S1070-6631(96)02511-1]

I. INTRODUCTION

Direct numerical simulation (DNS) has recently become an accessible approach for investigating complex phenomena in simple turbulent flows. Although simulated Reynolds numbers remain lower than those found in most practical applications, continued increases in computer power have made it possible to simulate many laboratory flows, such as grid turbulence or shear flow, at similar Reynolds numbers to those investigated experimentally. This opens up many opportunities for DNS to investigate quantities currently difficult or impossible to measure experimentally. In this study we consider turbulent transport and mixing in the presence of a mean scalar gradient.

In 1952 Corrsin[1] predicted that, in stationary isotropic turbulence with a uniform mean velocity in one direction, an imposed cross-stream mean temperature gradient maintains itself. Several grid turbulence experiments were then reported confirming this prediction, where a mean temperature gradient was produced by differentially heating the turbulence producing grid.[2–4] However, the evolution of the scalar variance, $\langle\phi^2\rangle$, was unclear since differentially heating the grid produces a cross-stream gradient in $\langle\phi^2\rangle$. Warhaft and Lumley[5] and Sirivat and Warhaft[6] introduced different methods of producing a mean temperature gradient in grid turbulence with better results. They found that $\langle\phi^2\rangle$ increases linearly with downstream distance, as predicted theoretically by Sullivan[7] and Durbin.[8] Homogeneous shear flow experiments have also been performed with a mean temperature gradient.[9,10]

Kerr[11,12] reported DNS results for a passive scalar in isotropic turbulence without a mean gradient, but a similar report for the scalar with a mean gradient has not yet been published. (A passive scalar is one that has no effect on the velocity field.) The DNS results of Ruetsch and Maxey[13,14] consider only the small-scale vorticity and passive scalar structures for the first several eddy turnover times (T_E) where the scalar field is still evolving and not statistically stationary. Pumir[15] also reports on a passive scalar DNS study with a mean gradient, but with a primary focus on the probability density functions (pdfs) of the scalar gradients.

In the present study direct numerical simulations are used to investigate a passive scalar in statistically homogeneous, isotropic, and stationary turbulence, with a mean scalar gradient in the y-direction. The purpose of this work is to consider a number of important questions left unanswered by experimental and DNS studies in the literature, with a motivation of later contrasting this passive scalar flow to one with reaction.

Recently it has been realized that the local isotropy central to Kolmogorov theory[16] and long understood for velocities does not appear to hold for a passive scalar. Sreenivasan states that ''statistical isotropy is not 'natural' or 'obvious' for the small-scale scalar field in a shear flow''.[17] This is evident in the persistent skewness of the scalar derivative in the direction of the mean gradient (henceforth $\partial\phi/\partial y$). Holzer and Siggia[18] performed a number of large, statistically stationary simulations of turbulence with a passive scalar and found a persistent skewness of $\partial\phi/\partial y$ at all Péclet numbers (up to Pe=2700). Their results are for synthetic turbulence (two dimensional (2-D) and with forcing). They observed a ramp-cliff type of structure in the Eulerian scalar

[a]Telephone: 607-255-9113; Fax: 607-255-1222; Electronic mail: overholt@mae.cornell.edu

 1070-6631/96/8(11)/3128/21/$10.00

TABLE I. Run parameters. Angle brackets $\langle\rangle$ denote the time-averaged stationary value.

Parameter	Tabulated	Run 32.3	Run 64.3	Run 128.3	Run 128.4	Run 256.5
N—grid size	N	32	64	128	128	256
n—number of simulations	n	16	16	4	4	1
ν—kinematic viscosity	ν	0.025	0.025	0.025	0.025	0.025
Pr—Prandtl number	Pr	0.7	0.7	0.7	0.7	0.7
β—mean scalar gradient $(d\langle\tilde{\phi}\rangle/dy)$	β	1.0	1.0	1.0	1.0	1.0
K_F—largest forced wave number	K_F/k_0	$2\sqrt{2}$	$2\sqrt{2}$	$2\sqrt{2}$	$2\sqrt{2}$	2
$k_{\max}$—largest resolved wave number	$k_{\max}\langle\eta\rangle$	1.120	1.107	1.121	1.133	1.060
k_0—smallest wave number	$k_0\langle\eta\rangle$	0.07422	0.03668	0.01859	0.01878	0.008786
$l\equiv\frac{1}{3}L_{i,i}$—integral length scale	$k_0\langle l\rangle$	1.259	1.091	0.9649	0.9696	1.378
$L_\epsilon\equiv u'^3/\epsilon$—turbulent length scale	$\langle L_\epsilon/l\rangle$	1.124	1.640	1.927	1.931	2.072
λ—Taylor microscale	$\langle\lambda/l\rangle$	0.6119	0.4761	0.3472	0.3484	0.1704
η—Kolmogorov length scale	$\langle\eta/l\rangle$	0.05893	0.03361	0.01926	0.01937	0.006374
T_E—eddy turnover time	$\langle l/u'\rangle$	1.396	0.4371	0.1540	0.1567	0.07028
τ_η—Kolmogorov time scale	$\langle\tau_\eta\rangle/T_E$	0.1580	0.1232	0.08981	0.0901	0.04397
T_s—start of the stationary period	T_s/T_E	5.923	6.142	4.595	14.08	4.698
T—duration of the stationary period	T/T_E	25.24	13.18	9.488	4.897	1.971
k—turbulent kinetic energy	$\langle k\rangle$	1.221	9.352	58.89	57.42	577.0
$u'\equiv(2k/3)^{1/2}$—turbulence intensity	u'	0.9024	2.497	6.266	6.187	19.61
v'—v-velocity rms value	$\langle v'\rangle$	0.8970	2.486	6.265	6.176	17.97
ϵ—dissipation	$\langle\epsilon\rangle$	0.5193	8.703	132.3	126.5	2641
$\mathrm{Re}_l\equiv u'l/\nu$—Reynolds number	$\langle\mathrm{Re}_l\rangle$	45.69	109.5	242.5	241.0	1092
$R_\lambda\equiv u'\lambda/\nu$—Taylor Reynolds number	$\langle R_\lambda\rangle$	27.84	51.93	83.94	83.69	185.0
$\langle v\phi\rangle$—scalar flux	$\langle v\phi\rangle$	−0.7726	−2.059	−4.749	−4.723	−13.31
$\langle\phi^2\rangle$—scalar variance	$\langle\phi^2\rangle$	2.027	2.179	2.019	1.891	2.488
ϕ'—scalar rms value	$\langle\phi^2\rangle^{1/2}$	1.424	1.476	1.421	1.375	1.577
$\mathrm{rms}(\partial\phi/\partial y)$—scalar gradient rms	$\langle(\partial\phi/\partial y)^2\rangle^{1/2}$	2.733	4.493	6.976	6.637	12.91
ϵ_ϕ—scalar dissipation	$\langle\epsilon_\phi\rangle$	0.7694	2.068	4.928	4.506	17.01
$r_\phi\equiv\epsilon_\phi/\langle\phi^2\rangle$—scalar dissipation rate	$\langle r_\phi\rangle$	0.3795	0.9490	2.441	2.383	6.837
$r\equiv 2k/\epsilon/\langle\phi^2\rangle/\epsilon_\phi$—time scale ratio	$\langle r\rangle$	1.822	2.080	2.215	2.216	3.038

field, which was shown by Sreenivasan *et al.*[19] to explain the skewness in the scalar derivative. This same structure was observed in the grid turbulence experiments of Tong and Warhaft[20] and in the atmospheric measurements of Phong-Anant *et al.*[21] Holzer and Siggia[18] show that this structure derives from the large scale organization of the scalar field, with large regions of fluid of relatively constant value being joined by steep ramps. Their conclusions have been generally confirmed at low Reynolds numbers by the DNS results of Pumir.[15] These results are all evidence that the passive scalar field is different from that which is predicted by the hypothesis of local isotropy and the Kolmogorov first similarity hypothesis.[16,17]

Kolmogorov's 1962 small scale intermittency extension to his original theory[22] inspired a number of local isotropy studies which found among other things that the pdf of the scalar derivative had ''stretched-exponential'' tails. But in 1989 the Chicago Rayleigh–Bénard convection experiment[23] ignited interest in the tails of the scalar pdf itself by showing that they could be exponential as well. It was proposed that there exists a universal threshold Rayleigh number $(\mathrm{Ra}\sim 4\times 10^7)$ across which the tails of the scalar pdf change from Gaussian to exponential. Jayesh and Warhaft[24] find this same transition at an integral-scale Reynolds number (Re_l) of about 70 in their grid turbulence experiments with a mean scalar gradient. Hence the terminology ''soft turbulence'' for turbulence below this critical Reynolds number (or Ra) where the scalar fluctuations are Gaussian, and ''hard turbulence'' for higher Reynolds number turbulence where the fluctuations are exponential.

Theoretical results were advanced by Pumir *et al.*[25] in the form of a very general one-dimensional (1-D) phenomenological model predicting exponential tails in the presence of a mean gradient. Kerstein[26] has shown that the linear-eddy model also yields scalar pdfs with exponential tails when there is a mean scalar gradient.

Several other experiments with mean scalar gradients have been done with mixed results. Thoroddsen and Van Atta[27] investigated stably stratified grid turbulence and found Gaussian scalar pdfs even when the scalar was passive. However, their maximum value of R_λ is 41, which according to Jayesh and Warhaft[24] is too small for exponential behavior. But that is not true of the turbulent shear flow results of Tavoularis and Corrsin.[9] They also observed Gaussian scalar pdfs in spite of R_λ being greater than 200.

Published DNS results on this topic have been minimal until recently, with all but one study observing only Gaussian pdfs. Kerr[11] performed stationary simulations for values of R_λ ranging from 9 to 83, and observed Gaussian pdfs; both the velocity and the scalar were forced. Eswaran and Pope[28] also performed stationary simulations with a forced velocity field and values of R_λ from 28 to 51, but they allow the scalar field to evolve from a double-delta pdf initial condition. They find that the evolving scalar pdf tends to a Gaussian. However, the first authors to formally address the case of a mean scalar gradient were Jaberi *et al.*[29] who made

a more comprehensive study of the scalar pdf tails and found that the long-time scalar pdf (at $R_\lambda = 58$) is not necessarily Gaussian or exponential, but rather is sensitive to several factors. If any forcing or a mean scalar gradient is present, then non-Gaussian behavior is not sustained for any initial conditions. Otherwise the scalar pdf is very sensitive to the initial conditions.

The scalar pdf is of interest not only for its own sake, but also because pdf methods are finding increased use for problems of turbulent mixing and reaction.[30,31] An emphasis of this study is the determination of statistics appearing in equations such as the scalar pdf transport equation. In this equation the conditional expectations $\langle v|\phi=\psi\rangle$ and $\langle \epsilon_\phi|\phi=\psi\rangle$ need to be modeled. (The conditional expectation $\langle v|\phi=\psi\rangle$, for example, is the expectation of v given that $\phi=\psi$, where v is the y-component of velocity and ψ is the scalar value; ϵ_ϕ is the scalar dissipation.) The grid turbulence experiments of Jayesh and Warhaft[24] and the DNS simulations of Eswaran and Pope[28] without a mean scalar gradient examine these conditional quantities for decaying turbulence. The paper by Miller *et al.*[32] gives some DNS results for the stationary case, but our results are the most comprehensive to date for stationary turbulence with a mean scalar gradient.

A great advantage of pdf methods is their closed-form, exact treatment of reaction and convection; however, mixing needs to be modeled. Almost all currently employed models for scalar mixing require information on the coupling between the turbulence time scale and the scalar dissipation time scale for closure.[33] One such relation is the mechanical-to-thermal time scale ratio, r. Another such relation is the scalar dissipation rate, which is a key quantity in the modeling of both inert and reactive turbulent scalar fields.[34] This coupling is examined in this paper via pdfs, joint pdfs, and conditional expectations of the turbulent and scalar dissipation.

These issues are investigated via DNS on grids ranging from 32^3 to 256^3, yielding values of R_λ from 28 to 185 (the Prandtl number is 0.7), a much larger range than has been considered before in three-dimensions. The largest velocity scales are forced to maintain stationarity. Multiple independent simulations (MIS) are performed for all but the largest grid size so that confidence intervals can be calculated. The large grid sizes and MIS are made possible by using from 16 to 64 processors in parallel on the IBM SP2 supercomputer.

The organization of the paper is as follows. In the following section the DNS algorithm and turbulent flow simulated are briefly described. In Sec. III some relevant statistics and the smoothing method are reviewed. Section IV describes and discusses the results, with comparison to experiment, and final conclusions and research directions are given in Sec. V.

II. METHOD

The DNS algorithm used is a fully parallelized version of the pseudo-spectral method of Rogallo.[35] In detail, the method used is almost identical to that used by Eswaran and Pope,[28] Yeung and Pope,[36] and Lee and Pope.[37] However, a completely new code has been written for distributed-memory message-passing architectures such as the IBM SP2. This is the same algorithm (without the particle tracking) as Yeung developed independently using MPL (IBM's Message Passing Library).[38] We use MPI (Message Passing Interface Standard).

The full Navier–Stokes and scalar equations are solved without modeling on a three-dimensional grid. The grid is a cube with sides of length 2π in physical space. In wave number space the grid represents the integer wave numbers

$$k_i = \pm n_i, \tag{1}$$

where $n_i = 0,1,2,\ldots,N/2$ for $i=1,2,3$. The pseudo-spectral method advances the solution in time in wave number space; however, the nonlinear products in the convection terms are formed in physical space, requiring discrete fast Fourier transforms (FFTs) to transform the fields back and forth between physical space and wave number space. The use of a Fourier representation imposes periodic boundary conditions in all three directions, and assures homogeneous fields.

The aliasing errors incurred in the FFTs are almost completely removed by phase shifting and truncation techniques.[35] The truncation results in a maximum significant wave number, $k_{\max}$, of $\sqrt{2}Nk_0/3$.

The time-stepping scheme is an explicit second-order Runge–Kutta method. Time-stepping errors are small as long as the Courant number, defined as

$$C = (|u|+|v|+|w|)_{\max}\frac{\Delta t}{\Delta x}, \tag{2}$$

is not greater than 1.0 (where u, v, and w are the three fluctuating velocities, Δt is the time step, and Δx is the grid spacing).[39] All the simulations in this study use the Courant number $C=0.8$. Table I provides a summary of the different simulations performed, and of the definitions and values of the primary quantities characterizing the flow.

The largest Reynolds number flow that can be accurately simulated for any grid size has been determined to be that for which the highest wave number $k_{\max}\eta \geqslant 1.0$, where η is the Kolmogorov length scale, the smallest length scale of the flow.[39] As can be seen in Table I, these simulations all have $k_{\max}\eta \approx 1.1$.

The velocity field is stochastically forced by adding acceleration increments to the largest scales only, such that continuity is satisfied and on average dissipation equals the artificial production. This results in the Reynolds number remaining relatively constant throughout each simulation. Only the wave numbers inside a sphere of radius K_F are forced (excluding the origin). This forcing introduces a forcing Reynolds number and time scale into the simulation that can be varied to give a flow of the desired Reynolds number and large scale size (integral length scale l). This forcing scheme is the same one used by Yeung and Pope,[36] a refinement of that developed and tested by Eswaran and Pope.[39] In these works it is shown that the resulting velocity fields are stationary and isotropic, to a good approximation.

The physically analogous turbulent flow is ''grid turbulence'' with one exception: grid turbulence is decaying (tur-

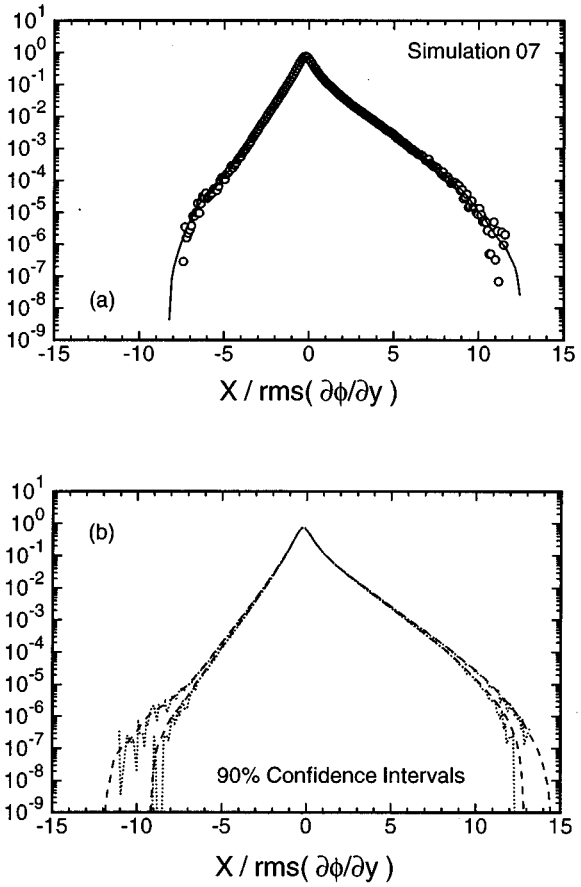

FIG. 1. Smoothing example for the pdf of $\partial\phi/\partial y$. X is the sample space variable, which is standardized by the rms of $\partial\phi/\partial y$. $R_\lambda = 52$; (a) raw data (symbols) and the smoothed result (line) for 1 of the 16 simulations; (b) confidence intervals based on 16 simulations: ⋯, unsmoothed; − −, smoothed.

bulent kinetic energy decreases downstream from the turbulence producing grid), whereas in our simulations the velocity fields are statistically stationary.

The scalar fluctuation equation (see Eq. (24)) is solved for the evolution of the passive scalar fluctuation, which is initially set to zero. No scalar forcing is necessary since the mean scalar gradient gives rise to a nonzero production term in the scalar variance evolution equation (see Eq. (15)). The initial mean scalar gradient is maintained because, for homogeneous turbulence, its evolution equation is

$$\frac{\partial}{\partial t}\left(\frac{\partial\langle\tilde{\phi}\rangle}{\partial x_i}\right) = 0. \tag{3}$$

For each simulation, the velocity field is initalized and allowed to evolve until it reaches stationarity (at least 4 eddy turnover times) so the effects of its initial condition are minimal. Then the scalar is introduced. After the scalar field is deemed to have reached stationarity, the simulation is carried on for 2 to 25 eddy turnover times, over which time interval statistics are averaged in time as well as in space.

The time required to compute 1 eddy turnover time on 1 SP2 processor is 0.019 hours for 32^3, and 0.37 hours for 64^3. For 128^3 split over 4 processors, the time required is 2.3 hours for each processor (a sum total of 9.2 hours); 256^3 split over 32 processors requires 12.8 hours each (410 hours total).

III. STATISTICS

Since turbulence is a stochastic process, each DNS simulation is by nature a stochastic simulation in that the results are random variables which depend on the initial condition. In addition, randomness enters the simulation through the stochastic forcing of the velocity field. Hence the idea of using MIS, which involves performing several statistically identical simulations with randomly different initial conditions. Using the IBM SP2 supercomputer, individual processors each perform one simulation, each with identical run parameters; the only differences between the simulations are the stochastic forcing and the initial fields, which are randomly specified according to the same distribution. Output from all the processors or simulations can then be combined to form means and confidence intervals.

In addition, for the larger simulations it becomes necessary to split up each simulation via domain-decomposition over several processors, both for memory and CPU time constraints. All this is very efficiently accomplished in parallel using MPI.

The use of MIS allows confidence intervals to be determined for every quantity desired, and they appear in many of the figures in this paper. Confidence intervals of 90% were chosen: for a random variable X, the confidence interval $[a,b]$ is such that $\mathrm{Prob}[a \leqslant X \leqslant b] = 0.90$. This is very useful for determining statistical significance. For instance, if two quantities are being compared and one lies inside the confidence interval of the other, then statistically the difference is

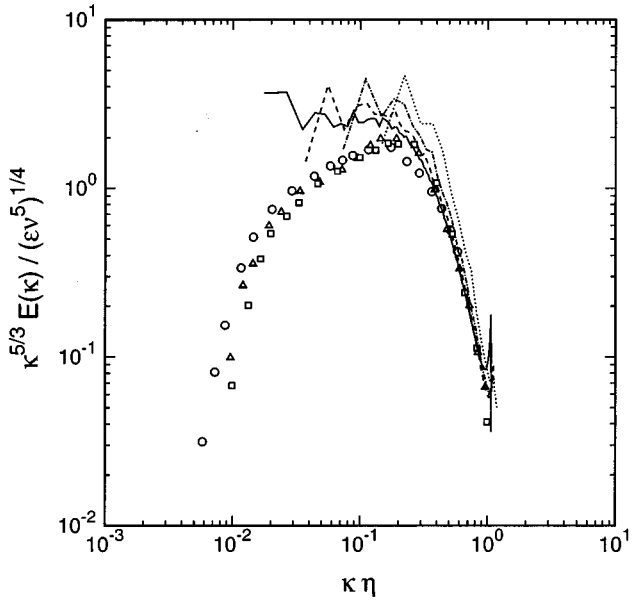

FIG. 2. Energy spectrum function from DNS (lines) and from the experiments of Comte-Bellot and Corrsin (symbols), scaled to show the $-5/3$ region. Values for R_λ are: ○, 71.6; △, 65.3; □, 60.7; —, 185; − −, 84; − · −, 52; ⋯, 28.

not significant. The difference is only significant if there is no overlap between the two confidence intervals.

Let n be the number of simulations. Then for some variable y_i from the ith simulation, the first two statistical moments, the sample mean and variance, are

$$\overline{y} = \frac{1}{n}\sum_{i=1}^{n} y_i, \tag{4}$$

$$s = \frac{1}{n-1}\sum_{i=1}^{n} (y_i - \overline{y})^2. \tag{5}$$

To form the confidence interval the Student-t distribution is used because the true variance is unknown; the calculated-variance is the sample variance. The Student-t distribution is a function of the number of degrees of freedom of the system, which here is the number of simulations. For an interval $[a,b]$ of the random variable X with Prob$[a \leqslant X \leqslant b] = 1-\alpha$ and n simulations, the Student-t confidence interval is

$$\left[\overline{y} - t_{\alpha/2,n-1}\frac{s}{\sqrt{n}}, \overline{y} + t_{\alpha/2,n-1}\frac{s}{\sqrt{n}}\right]. \tag{6}$$

The values of the coefficients used are $t_{0.05,3} = 2.3534$ and $t_{0.05,15} = 1.7530$.

In a histogram formed from the data, the largest statistical fluctuations are in the tails, which are formed by a few very rare events. A similar situation occurs for conditional expectations at their extremes (i.e., for the largest fluctuations of the random variable conditioned on). Since these quantities are central to this study, a smoothing technique is employed to further minimize the statistical fluctuations of the results.

The data are processed as follows. Individual histograms are output for each simulation (with time-averaging only within each respective simulation). Each histogram is then smoothed using a local regression procedure to be described. The smoothed histograms from each simulation are then combined to form smoothed means and confidence intervals. The sole difference between the processing of the smoothed results and the normal MIS results is the smoothing step.

The smoothing is accomplished via a local regression method developed by Ruppert.[40] Given a function $y = f(x)$ to be smoothed in the interval $[a,b]$ and then evaluated at the point $x_0 \in [a,b]$, a local regression smoother fits a low-order polynomial in the independent variable x locally at x_0, and then takes the estimate of $f(x_0)$ from the fitted polynomial at x_0. Local regression smoothers automatically avoid biases common to kernel smoothers. These biases can occur at the boundary of the predictor space since there the kernel neigh-

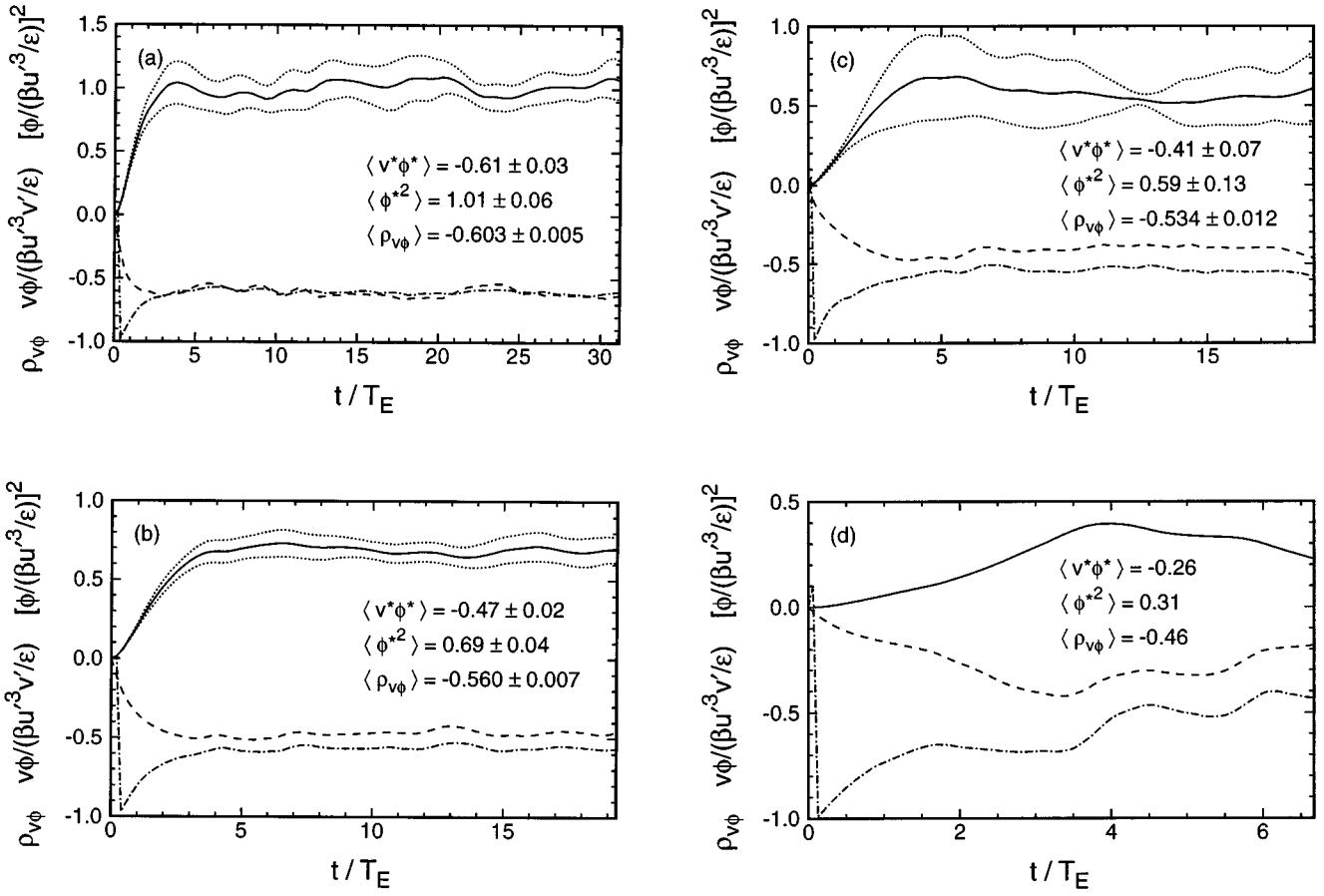

FIG. 3. Evolution of the normalized scalar variance, scalar flux and its correlation coefficient. —, $\langle(\phi^*)^2\rangle$; ⋯, confidence intervals on $\langle(\phi^*)^2\rangle$; − −, $\langle v^*\phi^*\rangle$; − · −, $\rho_{v\phi}$. (a) $R_\lambda = 28$; (b) $R_\lambda = 52$; (c) $R_\lambda = 84$; (d) $R_\lambda = 185$.

TABLE II. Normalized stationary scalar variance and scalar flux.

Variable	Run 32.3	Run 64.3	Run 128.3	Run 128.4	Run 256.5
$\langle\phi^2\rangle/(\beta L_\epsilon)^2$	1.012	0.6810	0.5838	0.5395	0.3052
$\langle\phi^2\rangle/(\beta l)^2$	1.279	1.831	2.169	2.011	1.310
$\langle v\phi\rangle/(v'\beta L_\epsilon)$	−0.6087	−0.4631	−0.4076	−0.4084	−0.2594
$\langle v\phi\rangle/(v'\beta l)$	−0.6842	−0.7593	−0.7856	−0.7887	−0.5375

borhood is asymmetric; they can occur in the interior as well if the data are nonuniform or has substantial curvature.[41] As well as avoiding bias, the local regression method of Ruppert automatically adjusts to the data itself, so that the width of the neighborhood of x_0 considered (bandwidth, or number of points for evenly spaced data) is continuously variable. The support is thereby kept small in the center of the pdfs where the variability of the data is small, and increased in the tails where the variability is large.

Figure 1 gives an example of smoothing for the pdf of $\partial\phi/\partial y$ from the 64^3 run. In Fig. 1(a) the original data and the resulting smoothed curve are shown for 1 of the 16 simulations. Figure 1(b) shows the confidence intervals obtained from all 16 simulations. In the center of the pdf the smoothed confidence interval curves fall on top of the unsmoothed curves, but in the tails the smoothed intervals are more uniform and a bit smaller. The sharp peak of this pdf is slightly rounded since the curvature is very high there, but otherwise the smoothing does not degrade the results in the center where the accuracy of the unsmoothed pdf is already good, and in the tails the smoothed result shows much less fluctuation with values that appear reasonable.

IV. RESULTS

A. Energy spectrum function

We begin the results discussion with the energy spectrum function to establish the validity of these simulations. Figure 2 shows the energy spectrum functions from the four simulations with a $-5/3$ Kolmogorov scaling, compared with the experimental data of Comte-Bellot and Corrsin.[42] The forcing of the large scales does significantly distort the DNS spectra at low wave numbers when compared with the experimental data; however, they approach a $-5/3$ scaling region, and the high wave number portions of the spectra match the experimental data very well. Since we are more interested in quantities which scale with the high wave number or dissipation range, the low wave number distortion is allowable. However, in the following discussions of the evolution of scalar variance and scalar flux the influence of the forcing must be remembered.

B. Evolution of the scalar field

The focus of this study is on the behavior of the scalar field; we begin with the lower-order moments. The mean of the scalar field is zero. The variance evolves from a zero initial value to a statistically stationary value after some period of time, as predicted by Corrsin.[1]

The convection-diffusion equation for a passive scalar $\tilde{\phi}$ is

$$\frac{\partial\tilde{\phi}}{\partial t}+\tilde{U}_j\frac{\partial\tilde{\phi}}{\partial x_j}=\Gamma\nabla^2\tilde{\phi}, \tag{7}$$

where Γ is the molecular diffusivity. After Reynolds decomposing the scalar and velocity into mean and fluctuating parts

$$\tilde{\phi}=\langle\tilde{\phi}\rangle+\phi, \tag{8}$$

$$\tilde{U}_i=\langle U_i\rangle+u_i, \tag{9}$$

with the conditions

$$\frac{\partial\langle\tilde{\phi}\rangle}{\partial t}=0, \tag{10}$$

$$\nabla^2\langle\tilde{\phi}\rangle=0, \tag{11}$$

the evolution equation for the scalar variance becomes

TABLE III. Reynolds stresses and scalar fluxes.

	Run 32.3	Run 64.3	Run 128.3	Run 256.5
$\langle u_1^2\rangle/u'^2$	+1.007±0.018	+1.006±0.025	+1.028±0.080	+1.075
$\langle u_2^2\rangle/u'^2$	+0.995±0.026	+0.995±0.022	+1.004±0.137	+0.845
$\langle u_3^2\rangle/u'^2$	+0.998±0.028	+0.999±0.037	+0.967±0.071	+1.080
$\langle u_1u_2\rangle/u'^2$	+0.009±0.011	−0.006±0.016	+0.023±0.038	+0.085
$\langle u_1u_3\rangle/u'^2$	−0.003±0.012	−0.015±0.015	−0.007±0.038	+0.027
$\langle u_2u_3\rangle/u'^2$	+0.013±0.018	+0.009±0.015	+0.018±0.028	−0.115
$\langle u_1\phi\rangle/u'\phi'$	−0.015±0.013	+0.008±0.019	−0.026±0.033	+0.023
$\langle u_2\phi\rangle/u'\phi'$	−0.601±0.030	−0.559±0.024	−0.533±0.094	−0.430
$\langle u_3\phi\rangle/u'\phi'$	−0.016±0.025	−0.012±0.018	−0.018±0.061	+0.206

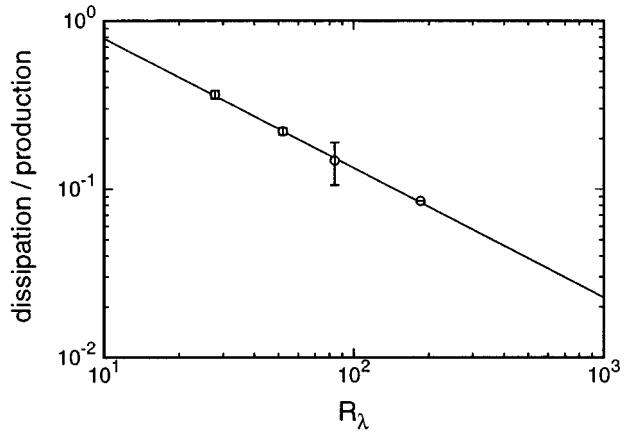

FIG. 4. Dissipation/production in the scalar flux equation. Error bars denote the 90% confidence intervals. The solid line corresponds to $4.61R_\lambda^{-0.769}$.

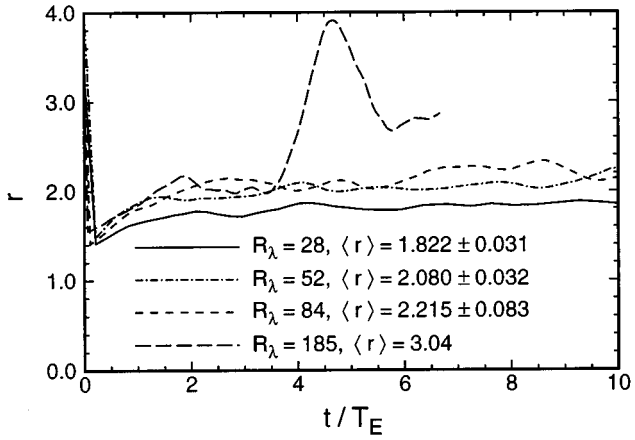

FIG. 5. Evolution of the mechanical-to-thermal time scale ratio.

$$\frac{1}{2}\frac{\partial}{\partial t}\langle\phi^2\rangle+\frac{\langle U_j\rangle}{2}\frac{\partial}{\partial x_j}\langle\phi^2\rangle$$
$$=-\langle u_j\phi\rangle\frac{\partial\langle\tilde{\phi}\rangle}{\partial x_j}-\frac{\partial}{\partial x_j}\left[\left\langle\frac{1}{2}u_j\phi^2\right\rangle-\frac{\Gamma}{2}\frac{\partial}{\partial x_j}\langle\phi^2\rangle\right]$$
$$-\Gamma\left\langle\frac{\partial\phi}{\partial x_j}\frac{\partial\phi}{\partial x_j}\right\rangle. \tag{12}$$

For homogeneous fields with the additional conditions

$$\langle U_i\rangle=0, \tag{13}$$

$$\frac{\partial\langle\tilde{\phi}\rangle}{\partial x_j}=\beta\delta_{j2}, \tag{14}$$

we get the scalar variance evolution equation for our study

$$\frac{1}{2}\frac{d}{dt}\langle\phi^2\rangle=-\langle v\phi\rangle\beta-\langle\epsilon_\phi\rangle, \tag{15}$$

where $v=u_2$ and the scalar dissipation is defined as

$$\epsilon_\phi\equiv\Gamma\left\langle\frac{\partial\phi}{\partial x_j}\frac{\partial\phi}{\partial x_j}\right\rangle. \tag{16}$$

Equation (15) indicates that for the scalar variance to be stationary, gradient production must be balanced by molecular dissipation.

Gradient production for the scalar variance comes from the scalar flux working against the mean gradient β; therefore, the scalar flux dynamics are important when considering the evolution of the scalar variance.

The scalar flux evolution equation is

$$\frac{\partial}{\partial t}\langle v\phi\rangle+\langle U_j\rangle\frac{\partial}{\partial x_j}\langle v\phi\rangle$$
$$=-\langle vu_j\rangle\frac{\partial\langle\tilde{\phi}\rangle}{\partial x_j}-\langle u_j\phi\rangle\frac{\partial\langle V\rangle}{\partial x_j}-\frac{\partial}{\partial x_j}\langle u_jv\phi\rangle$$
$$-\frac{1}{\rho}\left\langle\phi\frac{\partial p}{\partial y}\right\rangle+\Gamma\langle v\nabla^2\phi\rangle+\nu\langle\phi\nabla^2 v\rangle. \tag{17}$$

For homogeneous fields with the same conditions as above we get the scalar flux evolution equation for our study

$$\frac{\partial}{\partial t}\langle v\phi\rangle=-\langle v^2\rangle\beta-\frac{1}{\rho}\left\langle\phi\frac{\partial p}{\partial y}\right\rangle-(\nu+\Gamma)\left\langle\frac{\partial v}{\partial x_j}\frac{\partial\phi}{\partial x_j}\right\rangle, \tag{18}$$

where $y=x_2$. The terms on the right-hand side are production, pressure-scrambling, and dissipation. The dissipation term is often neglected on the grounds that it is zero if local

TABLE IV. Correlation coefficients.

Correlation	Run 32.3	Run 64.3	Run 128.3	Run 256.5
$\rho_1\equiv\rho(\partial\phi/\partial x,\partial v/\partial x)$	-0.447 ± 0.005	-0.310 ± 0.006	-0.219 ± 0.016	-0.124
$\rho_2\equiv\rho(\partial\phi/\partial y,\partial v/\partial y)$	-0.295 ± 0.005	-0.202 ± 0.005	-0.148 ± 0.012	-0.085
$\rho_3\equiv\rho(\partial\phi/\partial z,\partial v/\partial z)$	-0.448 ± 0.005	-0.310 ± 0.006	-0.218 ± 0.016	-0.124
$\rho_4\equiv\rho(\nabla\phi,\nabla v)$	-0.401 ± 0.004	-0.277 ± 0.005	-0.196 ± 0.014	-0.112
$\rho_5\equiv\rho(\partial\phi/\partial y,\partial u/\partial y)$	-0.009 ± 0.008	$+0.002\pm0.006$	-0.004 ± 0.012	$+0.000$
$\rho_6\equiv\rho(\partial\phi/\partial y,\partial u/\partial x)$	$+0.144\pm0.004$	$+0.101\pm0.004$	$+0.074\pm0.004$	$+0.043$
$\rho_7\equiv\rho(\partial\phi/\partial x,\partial u/\partial y)$	$+0.106\pm0.004$	$+0.074\pm0.003$	$+0.055\pm0.003$	$+0.031$
$\rho_8\equiv\rho(v,\phi)$	-0.603 ± 0.005	-0.560 ± 0.007	-0.534 ± 0.012	-0.464
$\rho_9\equiv\rho(u,\phi)$	-0.015 ± 0.013	$+0.008\pm0.019$	-0.022 ± 0.028	$+0.022$
$\rho_{10}\equiv\rho(\epsilon_\phi,\phi^2)$	-0.022 ± 0.004	-0.011 ± 0.006	-0.021 ± 0.010	-0.010
$\rho_{11}\equiv\rho(\partial\phi/\partial x,\partial\phi/\partial y)$	-0.003 ± 0.011	$+0.001\pm0.007$	-0.001 ± 0.011	-0.025
$\rho_{12}\equiv\rho(\partial u/\partial x,\partial u/\partial y)$	-0.005 ± 0.009	$+0.006\pm0.008$	-0.001 ± 0.012	$+0.000$

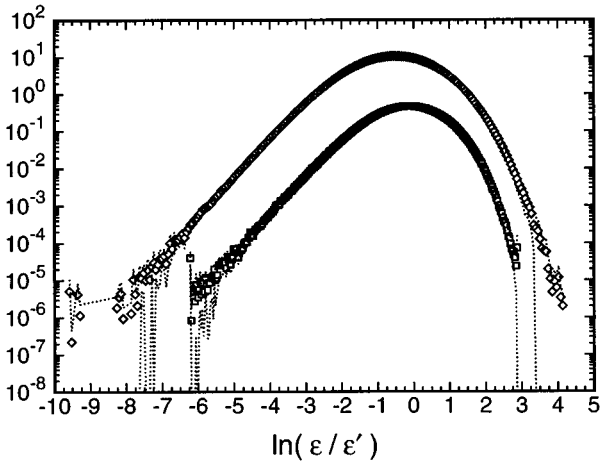

FIG. 6. Stationary pdf of the log of dissipation (mean plus fluctuation), $P[\ln(\epsilon/\epsilon')]$. □, $R_\lambda = 28$; ◇, $R_\lambda = 84$, shifted up two decades.

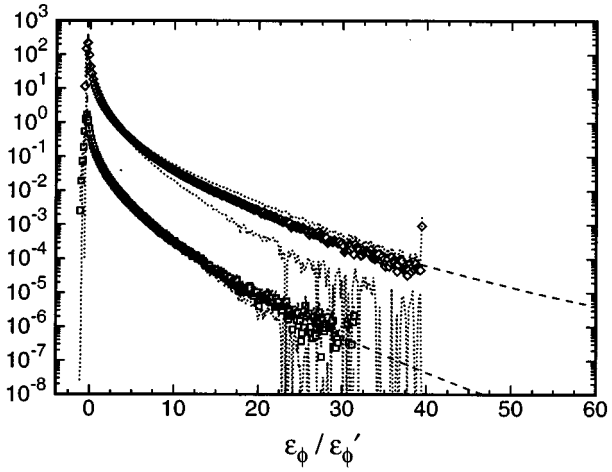

FIG. 8. Stationary standardized pdf of scalar dissipation, $P[X = \epsilon_\phi / \epsilon'_\phi]$. The dashed line is a stretched-exponential fit as in Fig. 7. □, $R_\lambda = 28$, $(\alpha_1, \alpha_2) = (1.59, 0.600)$; ◇, $R_\lambda = 84$, $(\alpha_1, \alpha_2) = (2.16, 0.469)$, shifted up two decades.

isotropy prevails, as is hypothesized at high Reynolds number.[6] We will examine this claim in more detail later.

Figure 3 shows the evolution of the nondimensionalized scalar variance, scalar flux and its correlation coefficient for each of the simulations ($\phi^* \equiv \phi/(\beta L_\epsilon)$, the normalized scalar fluctuation; for velocity we have $v^* \equiv v/v'$). Time is nondimensionalized by the eddy turnover time, and is set to zero at the time when the scalar fluctuations are initialized to zero. The solid line is the mean value and the dotted lines denote the limits of the 90% confidence intervals for the scalar variance. The mean value and confidence interval printed in each figure is the temporal average value for the stationary portion of each simulation (see Table I for the starting time, T_s, of the stationary portion of each simulation).

The only appropriate quantity available to normalize the scalar fluctuation is the mean scalar gradient, β. Hence an additional length scale is needed from the turbulence, and $L_\epsilon \equiv u'^3/\epsilon$ seems appropriate (see Table I). However, this normalization incurs a Reynolds number dependence. One could also use the integral length scale, l, to normalize. Table

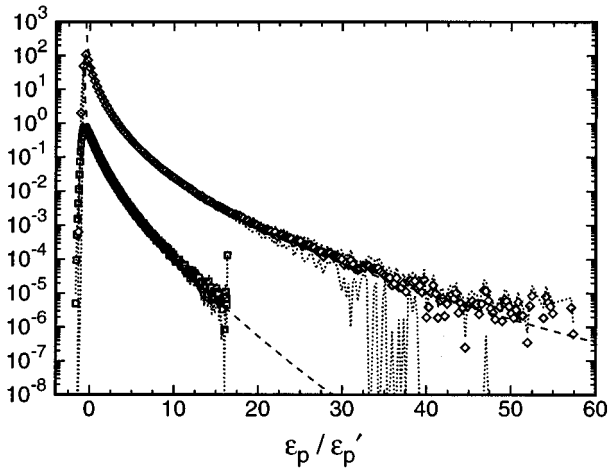

FIG. 7. Stationary standardized pdf of pseudo-dissipation, $P[X = \epsilon_p / \epsilon'_p]$. The dashed line is a stretched-exponential fit of the form (const) $X^{*-1/2}\exp[-\alpha_1 X^{*\alpha_2}]$, where $X^* = X - X_{\rm mp}$. □, $R_\lambda = 28$, $(\alpha_1, \alpha_2) = (1.48, 0.720)$; ◇, $R_\lambda = 84$, $(\alpha_1, \alpha_2) = (2.98, 0.450)$, shifted up two decades.

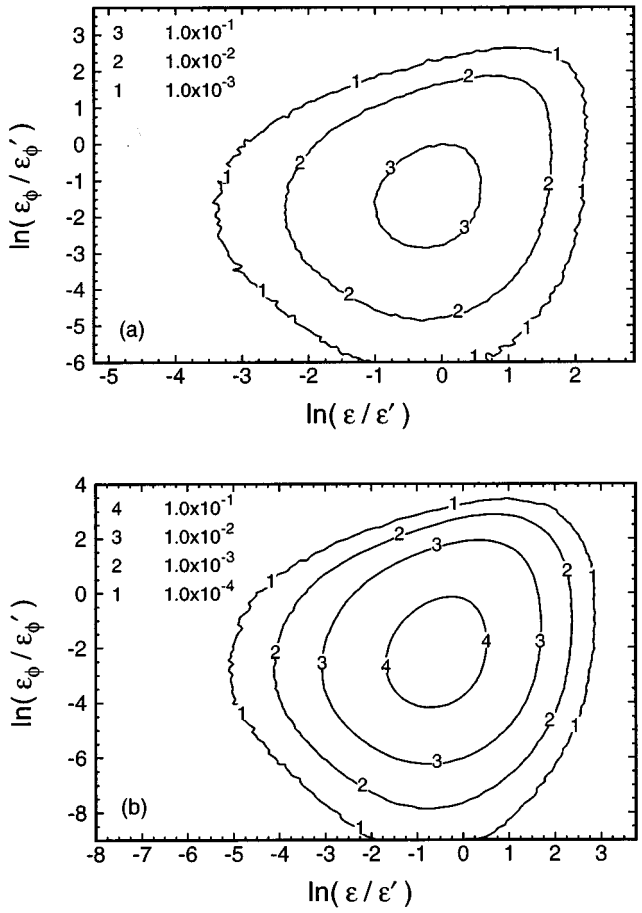

FIG. 9. Stationary joint pdf of $\ln(\epsilon_\phi/\epsilon'_\phi)$ vs $\ln(\epsilon/\epsilon')$. (The variables ϵ_ϕ and ϵ are the means plus the fluctuations.) (a) $R_\lambda = 28$; (b) $R_\lambda = 84$.

TABLE V. Stationary moments of the pdf of ϵ.

Moment	Run 32.3	Run 64.3	Run 128.4
Mean	0.519 ± 0.008	8.70 ± 0.20	$127. \pm 4$
Variance	0.211 ± 0.007	77.1 ± 3.6	$(2.02 \pm 0.15) \times 10^4$
Skewness	2.32 ± 0.03	2.97 ± 0.04	3.62 ± 0.12
Kurtosis	11.8 ± 0.4	19.0 ± 0.6	28.4 ± 2.6
Superskewness	499 ± 59	1740 ± 230	4900 ± 1440

II gives the stationary values of the scalar variance and the scalar flux normalized using both L_ϵ and l.

We see that in each simulation the scalar variance undergoes an initial transient for 3 to 4 eddy turnover times where it is growing, shortly after which it reaches stationarity. Once stationary, however, there is still a considerable amount of fluctuation. As a stochastic process some fluctuation is expected; however, the large extent of these fluctuations is most likely due to large fluctuations in the velocity scales from the forcing, which in turn affect the large scalar scales.

The evolution of the scalar flux in the same figures is qualitatively very similar to that of the scalar variance with both achieving stationarity at about the same time. Table III lists the stationary values for all the Reynolds stresses and scalar fluxes for these simulations.

The time scale for the evolution of the scalar variance and scalar flux is seen to be independent of Reynolds number; however, we have found it to be sensitive to l. As the Reynolds number increases l decreases (due to the forcing method employed) and the time to stationarity increases. This is one of the main reasons for decreasing K_F to 2 for the 256^3 run (a smaller forcing radius will result in a larger l).

C. Dissipation of scalar flux

It has been assumed that the dissipation term in the scalar flux evolution equation is negligible in flows with Reynolds numbers of this size or larger.[6] The destruction of scalar flux must then come from the pressure-scrambling term. To investigate this further, Fig. 4 shows the ratio of the mean dissipation term to the mean production term in the scalar flux evolution equation (Eq. (18)) for the stationary portions of the four runs. The pressure-scrambling term, which in the steady-state equals the difference between production and dissipation, was not calculated.

It can be seen that the ratio of dissipation to production does indeed decrease towards zero as Reynolds number increases; however, it is not negligible at these Reynolds numbers. The dependence with R_λ is approximately represented by a power law with exponent -0.77, which corresponds to the curve in the figure. Extrapolating from this data, for the dissipation to be less than 5% of the production, an R_λ of 350 would be required.

This decrease in importance of dissipation is also seen in the decrease of the correlation coefficient ρ_4 in Table IV.

TABLE VI. Stationary moments of the pdf of ϵ_p.

Moment	Run 32.3	Run 64.3	Run 128.4
Mean	0.519 ± 0.008	8.70 ± 0.20	127 ± 4
Variance	0.196 ± 0.007	82.9 ± 4.1	$(2.32 \pm 0.18) \times 10^4$
Skewness	2.64 ± 0.04	3.73 ± 0.08	4.68 ± 0.13
Kurtosis	15.53 ± 0.7	31.2 ± 1.8	49.4 ± 3.8
Superskewness	1020 ± 150	6350 ± 1260	$(1.75 \pm 0.42) \times 10^4$

TABLE VII. Parameters of Eq. (23) with $X = \epsilon / \epsilon'$.

$P[X^*]$	Run 32.3	Run 64.3	Run 128.4
α_1	1.38	2.30	2.81
α_2	0.778	0.584	0.500

D. Mechanical-to-thermal time scale ratio

An often considered time scale ratio is the mechanical dissipation to thermal (or scalar) dissipation ratio, usually denoted by r

$$r = \frac{2k/\epsilon}{\langle \phi^2 \rangle / \epsilon_\phi}, \tag{19}$$

which relates the large-scale time scales of the velocity and scalar fields. Although it has been suggested that this ratio be taken as a universal constant for modeling purposes,[43] there is now considerable evidence to show that it does not take on a universal value,[5,44,45] including our results.

Figure 5 shows the evolution of r for the first 10 eddy turnover times in each of the four runs. Note that r reaches stationarity after 2 or 3 eddy turnover times, which is before the scalar variance and scalar flux reach stationarity (see Fig. 3). (The large bump in the r value for $R_\lambda = 185$ is due to a large surge in the forcing energy input. Since there is only one simulation for this case, that fluctuation is not averaged out.)

Evidently there is a statistically significant increase in r with Reynolds number, which lends further support to the belief that r is flow dependent. The kinetic energy, k, is of course directly affected by the artificial forcing, and so the values of r obtained here may also be influenced by the forcing. However, they are well within the range of values reported by other researchers. Sirivat and Warhaft[6] found in their grid turbulence experiments that r tended to decrease downstream as the Reynolds number decreased, with approximate values of 1.2 to 2.0. Warhaft and Lumley[5] review a number of heated grid experiments and find r values of 0.6 to 2.4.

E. Dissipation and the scalar dissipation rate

The scalar dissipation rate is a key quantity in the modeling of both inert and reactive turbulent scalar fields.[34] Almost all currently employed models for scalar mixing, rang-

TABLE VIII. Parameters of Eq. (23) with $X = \epsilon_p / \epsilon_p'$.

$P[X^*]$	Run 32.3	Run 64.3	Run 128.4
α_1	1.48	2.52	2.98
α_2	0.720	0.517	0.450

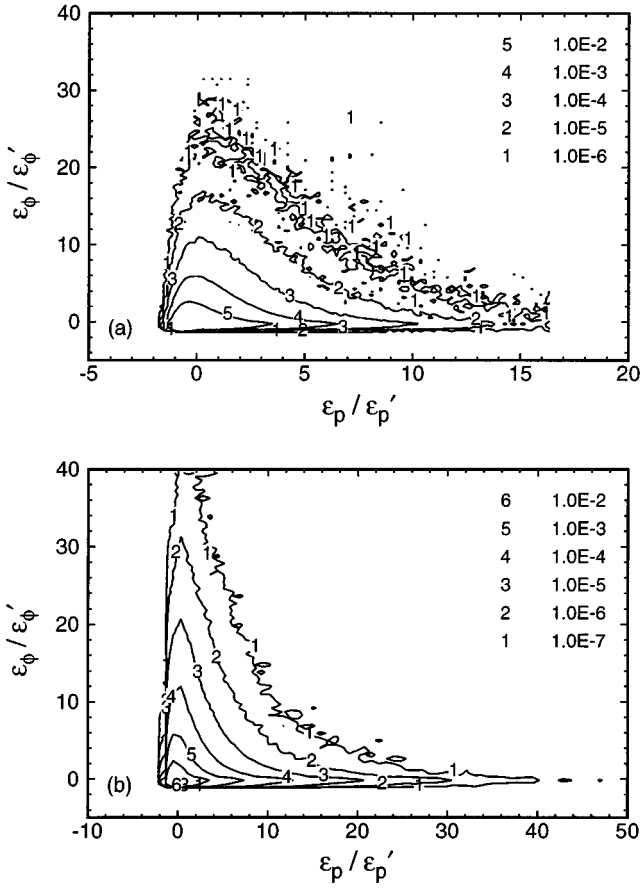

FIG. 10. Stationary standardized joint pdf of ϵ_ϕ vs ϵ_p (means plus fluctuations). (a) $R_\lambda = 28$; (b) $R_\lambda = 84$.

ing from simple moment closures to full pdf closures, require information concerning the coupling between the turbulence time scale and the scalar dissipation time scale for closure.[33] The mechanical-to-thermal time scale ratio gives one such relationship between the turbulence and the scalar, and as just seen it varies widely according to the flow under consideration. The scalar dissipation rate is another such relation, and is defined by

$$r_\phi = \frac{\epsilon_\phi}{\langle \phi^2 \rangle}. \tag{20}$$

In this section we present a number of statistics involving the turbulent dissipation and the scalar dissipation (which by inference includes the scalar dissipation rate).

1. Turbulent dissipation

Turbulent dissipation is defined, according to the turbulent kinetic energy equation, as

$$\epsilon = 2\nu s_{ij} s_{ij} = 2\nu \left[\frac{1}{2}\left(\frac{\partial u_i}{\partial x_j} + \frac{\partial u_j}{\partial x_i} \right) \right] \left[\frac{1}{2}\left(\frac{\partial u_i}{\partial x_j} + \frac{\partial u_j}{\partial x_i} \right) \right]. \tag{21}$$

A related quantity, often called the ''pseudo-dissipation,'' is

TABLE IX. Parameters of Eq. (23) with $X = \epsilon_\phi / \epsilon_\phi'$.

$P[X^*]$.	Run 32.3	Run 64.3	Run 128.4
α_1	1.59	1.78	2.16
α_2	0.600	0.546	0.469

$$\epsilon_p = \nu \frac{\partial u_i}{\partial x_j} \frac{\partial u_i}{\partial x_j}. \tag{22}$$

Pseudo-dissipation is easier to calculate and hence is often used in application, since in homogeneous turbulence mean dissipation equals mean pseudo-dissipation. However, as seen in Yeung and Pope,[36] other statistics of these two quantities are quite different, and for that reason both are presented in this paper.

Dissipation can also be calculated from the spectrum; however, to construct the pdf and conditional expectations of dissipation a local (in space) evaluation of dissipation is required. Hence Eqs. (21) and (22) are used to find the dissipation at each grid point.

The stationary moments of the pdfs of dissipation and pseudo-dissipation are given in Tables V and VI. Figure 6 shows the pdfs of $\ln(\epsilon/\epsilon')$ for $R_\lambda = 28$ and 84, with confidence intervals. (The confidence intervals for the largest values of the independent variable are of zero size because there was only one simulation which had a value for that bin.) The pdfs of ϵ_p / ϵ_p' are shown in Fig. 7 to emphasize the stretched-exponential nature of the tails (the pdfs of $\ln(\epsilon_p/\epsilon_p')$ are very similar to the pdfs of $\ln(\epsilon/\epsilon')$). All show the same Reynolds number dependence; as Reynolds number increases, the range of the standardized variable increases and the pdf tail lifts (or becomes stronger stretched exponential).

The stretched-exponential nature of the scalar gradient pdf tails (seen in Sec. IV H.) suggests that the dissipation pdf might be stretched exponential as well. Holzer and Siggia[18] find that for large X the dissipation pdf is approximated by a stretched exponential of the form

$$P[X] \sim C X^{-1/2} \exp(-\alpha_1 X^{\alpha_2}), \tag{23}$$

where α_1 and α_2 are parameters, and C is a constant. This expression also fits our data well (see Figs. 7 and 8), and serves to quantify the dissipation pdfs. The parameters for these and other fits are shown in Tables VII–IX. The lifting of the pdf tail is clearly seen in the decrease of α_2 as Reynolds number increases, a phenomenon which occurs for both the turbulent and the scalar dissipation. (Note: For the stretched-exponential fits the function plotted is $C X^{*-1/2} \exp(-\alpha_1 X^{*\alpha_2})$, where $X^* = X - X_{\rm mp}$, $X_{\rm mp}$ being the most probable value of X—where $P[X]$ is peaked.)

2. Scalar dissipation

The stationary moments of the scalar dissipation pdfs are given in Table X. Figure 8 shows the pdfs of $\ln(\epsilon_\phi/\epsilon_\phi')$ for $R_\lambda = 28$ and 84. At the smallest Reynolds number the pdf tail of scalar dissipation is lifted higher than either of the turbulent dissipation pdf tails (see Tables VII–IX). For the larger Reynolds numbers, α_2 for ϵ_p is similar to the value for ϵ_ϕ; however, the value of α_2 for ϵ is larger. In summary, all

TABLE X. Stationary moments of the pdf of ϵ_ϕ.

Moment	Run 32.3	Run 64.3	Run 128.4	Run 256.5
Mean	0.768 ± 0.035	2.07 ± 0.09	4.50 ± 0.76	17.05
Variance	1.75 ± 0.18	17.7 ± 1.7	115 ± 44	2080
Skewness	4.28 ± 0.07	5.44 ± 0.12	6.89 ± 0.61	8.14
Kurtosis	31.5 ± 1.2	51.5 ± 2.9	84.2 ± 16.8	117
Superskewness	3200 ± 370	$(1.01 \pm 0.21) \times 10^4$	$(2.86 \pm 1.22) \times 10^4$	6.04×10^4

of the dissipation pdfs have qualitatively the same shape, with the same kind of Reynolds number dependence.

We are now prepared to consider how scalar dissipation is correlated to the mechanical turbulent dissipation and pseudo-dissipation. We examine the joint pdfs and correlation coefficients to begin to answer this question.

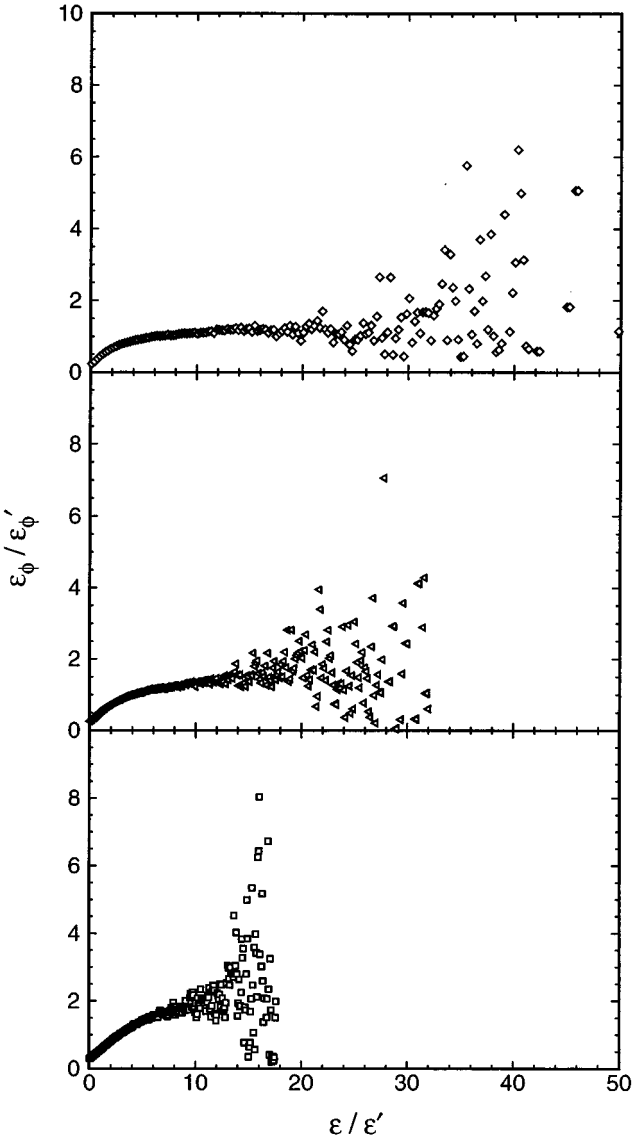

FIG. 11. Stationary conditional expectation of scalar dissipation given the mechanical dissipation (means plus fluctuations), $\langle \epsilon_\phi | \epsilon \rangle$. □, $R_\lambda = 28$; ◁, $R_\lambda = 52$; ◇, $R_\lambda = 84$.

Joint pdf contour plots of $\ln(\epsilon_\phi / \epsilon_\phi')$ vs $\ln(\epsilon/\epsilon')$ are shown in Fig. 9. (Note that the contour levels have exponential spacing.) It is evident that the contours for both Reynolds numbers differ from the ellipses of joint-lognormal random variables, and have a small but significant positive correlation.

For the dependence of the scalar dissipation on pseudo-dissipation the standardized joint pdf is shown in Fig. 10 (the joint pdfs of ϵ_ϕ vs ϵ and ϵ_ϕ vs ϵ_p are almost identical). This figure shows that the mechanical dissipation is inhibited by large values of scalar dissipation (and vice versa to a lesser degree), since the contours are concave and have sharp points at near zero scalar dissipation. This inhibition may be increasing slightly with Reynolds number, while the actual correlation as given in Table XI is decreasing.

Now that we have examined the correlation between scalar and mechanical dissipation via joint pdfs, we conclude with an examination of the conditional expectation $\langle \epsilon_\phi | \epsilon \rangle$.

Figure 11 gives the conditional expected value of scalar dissipation given the full mechanical dissipation. Results for three Reynolds numbers are shown because there is some Reynolds number dependence. The behavior at each Reynolds number is similar, but not identical. Each plot begins with an approximately linear departure from zero, increasing to a maximum with little statistical variability, after which the values quickly gain considerable variability.

Figure 12 gives similar results for the conditional expected scalar dissipation given the mechanical pseudo-dissipation; however, the behavior has some distinct differences. For one, the conditional expected value has a steeper slope near zero and levels off much quicker (at a smaller mechanical dissipation value), after which it begins to decrease before scattering out. This phenomenon becomes more apparent as Reynolds number increases. Also, the maximum value attained is only about one-half the maximum value in Fig. 11 for the full mechanical dissipation.

F. Modeled quantities in pdf evolution equations

The pdf approach is finding more and more use for practical computations of turbulence, especially for turbulent combustion. It has the great advantage of being able to treat

TABLE XI. Correlation coefficients for dissipation.

Correlation	Run 32.3	Run 64.3	Run 128.4
$\rho_{13} \equiv \rho(\epsilon, \epsilon_\phi)$	0.235 ± 0.004	0.189 ± 0.004	0.165 ± 0.013
$\rho_{14} \equiv \rho(\epsilon_p, \epsilon_\phi)$	0.124 ± 0.004	0.0877 ± 0.0035	0.0777 ± 0.0130

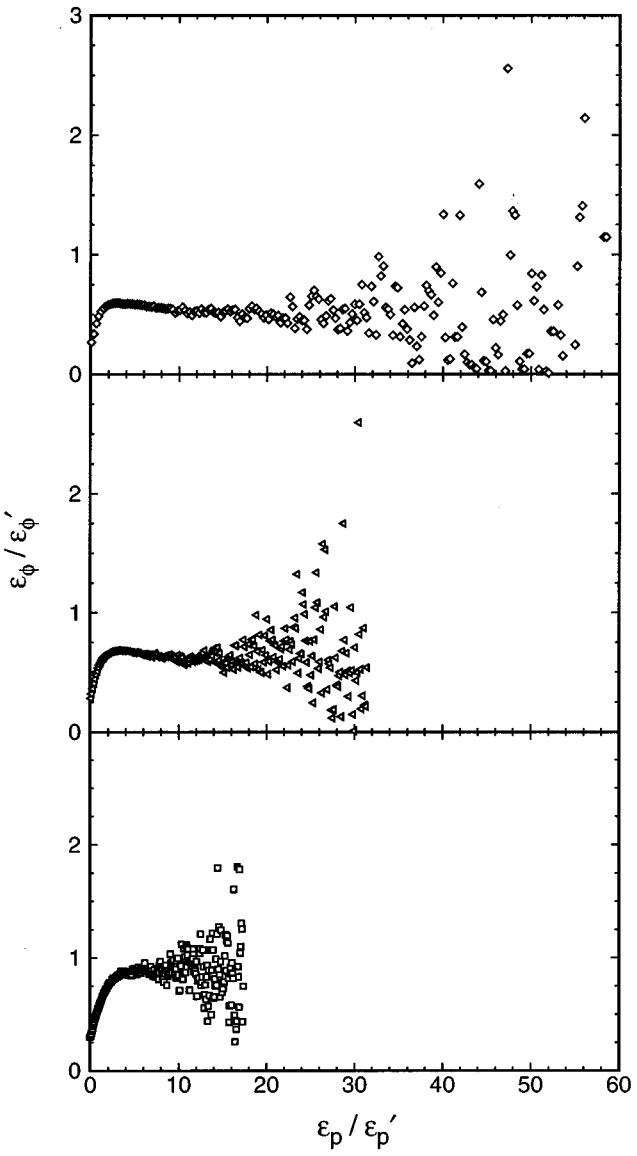

FIG. 12. Stationary conditional expectation of scalar dissipation given the mechanical pseudo-dissipation (means plus fluctuations), $\langle \epsilon_\phi | \epsilon_p \rangle$. □, $R_\lambda = 28$; ◁, $R_\lambda = 52$; ◇, $R_\lambda = 84$.

the convection and reaction processes exactly; models based on the assumption of gradient diffusion are not needed, and treatment of arbitrarily complex finite-rate reactions is possible. The ability to treat convection and reaction exactly alleviates many of the difficulties encountered in the Reynolds-stress approach; however, the pdf method is not without its own set of unclosed terms which need to be modeled.

1. Conditional scalar dissipation and velocity

One such pdf evolution equation, which applies to this study, is the scalar pdf equation. This equation in an Eulerian frame is derived as follows. We begin again with the convection-diffusion equation for a passive scalar, Eq. (7). Reynolds decomposing the scalar and velocity into mean and fluctuating parts with the previously given conditions, Eqs. (10), (13)–(14), gives the scalar fluctuation equation

$$\frac{\partial \phi}{\partial t} + v\beta + \frac{\partial}{\partial x_j}(u_j \phi) = \Gamma \nabla^2 \phi. \tag{24}$$

(For this equation, the gradients of the scalar flux in x and z are zero by symmetry, and the gradient of the scalar flux in y is neglected on the assumption that v and ϕ are jointly homogeneous.)

From this equation we can infer the governing equation for the pdf of the scalar.[34] Assuming homogeneity and stationarity of the pdf gives

$$0 = \beta \frac{d}{d\psi}(f\langle v|\psi\rangle) - \frac{d^2}{d\psi^2}(f\langle \epsilon_\phi|\psi\rangle), \tag{25}$$

where $\langle a|\psi\rangle$ signifies $\langle a|\phi(\mathbf{x},t)=\psi\rangle$ for any quantity a.

An explicit solution to this equation can be found. Integrating once we obtain

$$C_1 = -\beta f\langle v|\psi\rangle + \frac{d}{d\psi}(f\langle \epsilon_\phi|\psi\rangle). \tag{26}$$

As ψ tends to infinity, each term on the right hand side of Eq. (26) tends to zero, so that the integration constant C_1 is zero.

Integrating again we obtain

$$f(\psi) = \frac{C}{\langle \epsilon_\phi|\psi\rangle} \exp\left(\int_0^\psi \frac{\beta\langle v|\psi'\rangle}{\langle \epsilon_\phi|\psi'\rangle} d\psi' \right). \tag{27}$$

This is the general solution for the homogeneous, stationary scalar pdf, $f(\psi)$. The constant C is determined by the normalization condition $\int_{-\infty}^{\infty} f(\psi)d\psi = 1$.

This equation is in the form of the result of Pope and Ching,[46] and hence we know two sufficient conditions for this pdf to be Gaussian:

$$\langle \epsilon_\phi|\psi\rangle = \langle \epsilon_\phi\rangle, \tag{28}$$

$$\langle v|\psi\rangle = \frac{-\psi}{\beta\langle \epsilon_\phi\rangle}. \tag{29}$$

Figure 13 shows the nondimensionalized scalar dissipation conditioned on the scalar for one Reynolds number, typical of all the simulations. We see that for the large center portion the curve is nearly constant as required in the first condition above, Eq. (28), and at the correct value. However, for large ψ it seems to droop down towards zero (although there is substantial statistical uncertainty in these tails).

In the experiments of Jayesh and Warhaft[24] with decaying grid turbulence and exponential scalar pdf tails, a rounded V-shape is seen for the conditional scalar dissipation, persisting as the Reynolds number decays and similar in shape to that found by Eswaran and Pope[28] in their DNS simulations without a mean scalar gradient, after the initial transient. In those DNS simulations the scalar field was initialized as a double-delta pdf, and decayed to a Gaussian.

Miller *et al.*[32] have proposed and demonstrated that the shape of the conditional scalar dissipation depends on the shape of the scalar pdf. If the scalar pdf has Gaussian tails, then the conditional scalar dissipation has a flat shape, independent of ψ, as seen in our analysis. For exponential tails, the conditional scalar dissipation has a sharp V-shape. This

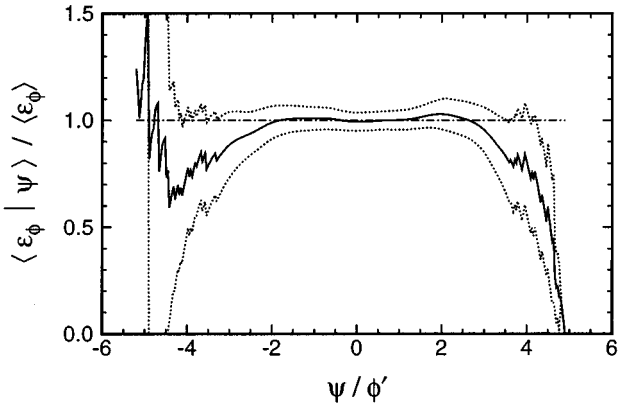

FIG. 13. Stationary scalar dissipation conditioned on the scalar. ψ is the sample space variable for ϕ. $R_\lambda = 52$; $-\cdot-$, Eq. (28).

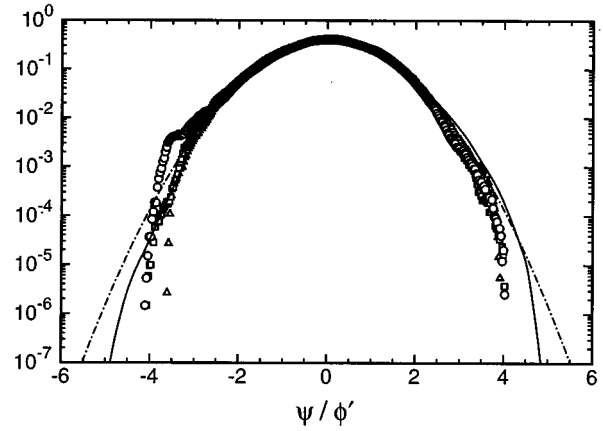

FIG. 15. Evolution of the scalar pdf to stationarity. (Note: Each curve is normalized by its respective instantaneous scalar rms value.) $R_\lambda = 84$; $\triangle$, $0.39T_E$; $\square$, $1.15T_E$; $\bigcirc$, $2.74T_E$; —, stationary pdf; $-\cdot-$, Gaussian.

is reminiscent of the results of Sahay and O'Brien,[47] who predicted similar shape dependencies based on a model for $\langle v|\psi\rangle$. Since, as will be seen, the scalar pdf tails in this study are at least quite close to Gaussian, the nearly flat shapes observed here for the conditional scalar dissipation agrees both with the above theories and with our analysis, at least for moderate values of ψ.

In examining these conditional quantities it is helpful to consider the appropriate correlation coefficients as well. As expected, the correlation ρ_{10} (see Table IV) between the scalar dissipation and the scalar variance is very small for all Reynolds numbers. However, considering the entire ψ-range of the figures (and the drooping of the tails) it is questionable how accurate the first condition, Eq. (28), is in general for this flow.

The normalized conditional v-velocity is shown in Fig. 14. In contrast to the conditional scalar dissipation, the confidence intervals are very small for this quantity. There is a clear almost linear dependence on the scalar, with a slope of -1, corresponding to the second condition, Eq. (29). The results for this quantity from the other simulations are very similar with a slope of minus one as well. The appropriate correlation coefficient in Table IV, ρ_8, is in the range $[-0.60,-0.46]$ and becoming smaller with Reynolds number.

Although the center portion of the stationary scalar pdf should be very close to Gaussian based on these results, the state of this pdf's tails is still in question. This question is examined in some detail later in this paper; we only consider it very briefly here.

Figure 15 details the evolution of the scalar pdf for $R_\lambda = 84$, characteristic of all of the simulations. (These transient curves and those following are not smoothed.) It begins as a delta function at zero (not shown) and then very quickly becomes Gaussian. Hence all the curves shown, each normalized by its respective scalar variance value, are Gaussian to a good approximation. (Although the confidence intervals are not shown in these figures for clarity, the Gaussian curve is inside the confidence interval of almost every point in each pdf.) Moments for the stationary scalar pdfs are given in Table XII.

If one considers the transient shapes of the conditional scalar dissipation, shown in Fig. 16, one sees a shape similar to the stationary shape (Fig. 13), rising in value as the scalar dissipation increases in response to the scalar variance. The

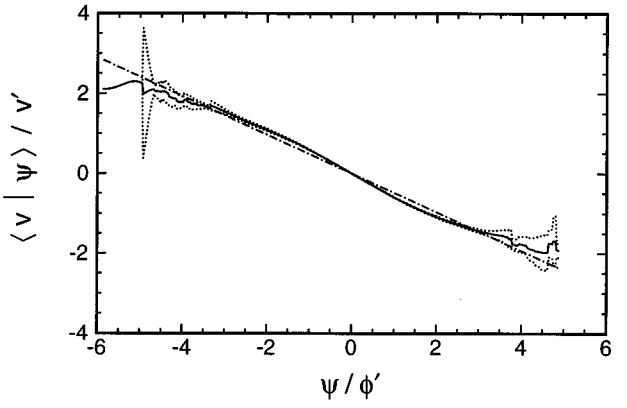

FIG. 14. Stationary v-velocity conditioned on the scalar. $R_\lambda = 52$; $-\cdot-$, Eq. (29).

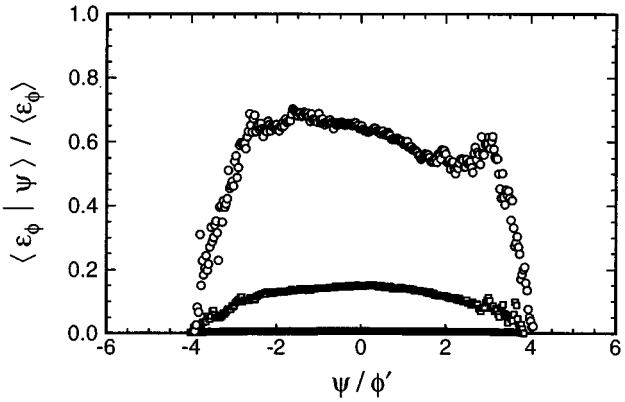

FIG. 16. Evolution of the scalar dissipation conditioned on the scalar. (See note in Fig. 15.) $R_\lambda = 52$: $\triangle$, $0.40T_E$; $\square$, $1.26T_E$; $\bigcirc$, $2.60T_E$.

TABLE XII. Stationary moments of the scalar pdf.

Moment	Run 32.3	Run 64.3	Run 128.3	Run 256.5
Mean	0.000 ± 0.000	0.000 ± 0.000	0.000 ± 0.000	0.000
Variance	2.020 ± 0.120	2.181 ± 0.123	2.032 ± 0.475	2.537
Skewness	-0.022 ± 0.031	0.008 ± 0.045	0.067 ± 0.072	0.159
Kurtosis	2.903 ± 0.031	2.976 ± 0.072	2.860 ± 0.097	3.171
Superskewness	13.60 ± 0.38	14.70 ± 1.05	13.08 ± 1.20	16.85

qualitative behavior or shape begins as a bit concave downward, but soon assumes the stationary shape. The associated transient correlation coefficients at these times are shown in Table XIII. They are fairly constant at a small negative value very close to the stationary value.

The transient shapes of the conditional v-velocity are shown in Fig. 17. Here we see a change in behavior as the scalar evolves. Since the v-velocity variance is already stationary when the scalar is introduced, the ratio of v-velocity variance to scalar variance changes as the scalar evolves, thereby affecting the slope. There is also an increased range in the conditional v-velocity when the scalar variance is small. This shows that the furthest excursions of the scalar early on are more closely correlated to the largest v-velocity fluctuations, which is mirrored in the transient correlation coefficient values (see Table XIII). From Eq. (24), at time dt immediately after the scalar is initialized, $\phi = -v\beta dt$, hence ϕ and v are perfectly correlated.

2. Scalar mixing

For the stationary case, an alternative form of the scalar pdf equation is

$$\beta(f\langle v|\psi\rangle) = \Gamma[f\langle \nabla^2\phi|\psi\rangle]. \tag{30}$$

The scalar mixing term $\langle \nabla^2\phi|\psi\rangle$ in this equation needs modeling, and is of much interest.[34] In the case of the velocity-scalar composition equation, the corresponding term to be modeled is

$$\Gamma\langle \nabla^2\phi|\mathbf{u},\psi\rangle. \tag{31}$$

This leads to the fundamental question ''What does scalar mixing depend on?'' Figure 18 shows the dependence of $\nabla^2\phi$ on the scalar value for two of the simulations. Both show a linear relationship with a slope of minus one. Figure 19 shows a similar linear relationship with v-velocity; however, here there is a Reynolds number dependence. The slope for $R_\lambda = 28$ is about 0.33, and for $R_\lambda = 52$ it is about 0.23. (The remaining simulations have slopes of 0.15 for $R_\lambda = 84$, and 0.083 for $R_\lambda = 185$.) Figure 20 shows contours of the dependence of $\nabla^2\phi$ on both the scalar and v-velocity, overlayed with the straight contour lines given by the model to be described. There is a large center planar region in the plot shaped like an ellipse and oriented at an angle to both axes, falling off to exponential spikes at the edges of the accessed (ϕ, v) space.

TABLE XIII. Transient correlation coefficients for 64^3, $R_\lambda = 52$.

Correlation	$0.40T_E$	$1.26T_E$	$2.60T_E$
$\rho_8 \equiv \rho(v,\phi)$	-0.969 ± 0.002	-0.758 ± 0.018	-0.630 ± 0.013
$\rho_{10} \equiv \rho(\epsilon_\phi, \phi^2)$	-0.029 ± 0.011	-0.041 ± 0.008	-0.021 ± 0.012

TABLE XIV. Model coefficients for Eq. (32).

Run	a	b
32.3	-1.231	-0.384
64.3	-1.268	-0.478
128.4	-1.310	-0.561
256.5	-1.229	-0.493

A model for these data can be formulated as

$$\frac{\nabla^2\phi}{\langle \epsilon_\phi\rangle/(\Gamma\phi')} = a\frac{\phi}{\phi'} + b\frac{v}{v'} + \xi, \tag{32}$$

where ϕ' is the scalar rms value, v' is the v-velocity rms value, and ξ is a zero-mean random variable uncorrelated with v and ϕ. Now let $\Phi \equiv \phi/\phi'$ and $V \equiv v/v'$, so that Eq. (32) can be written as

$$\frac{\nabla^2\Phi}{\langle \nabla\Phi\cdot\nabla\Phi\rangle} = a\Phi + bV + \xi. \tag{33}$$

Multiply by Φ and take the mean for

$$-1 = a + b\rho_{v\phi}. \tag{34}$$

Now multiply Eq. (33) by V and take the mean to get

$$\begin{aligned} a\rho_{v\phi} + b &= \frac{-\langle \nabla V\cdot\nabla\Phi\rangle}{\langle \nabla\Phi\cdot\nabla\Phi\rangle} \\ &= -\rho_{\nabla\phi,\nabla v}\left[\frac{\langle \nabla V\cdot\nabla V\rangle}{\langle \nabla\Phi\cdot\nabla\Phi\rangle}\right]^{1/2} \\ &= -\rho_{\nabla\phi,\nabla v}\left[\frac{\phi'^2\langle \epsilon\rangle}{2Prk\langle \epsilon_\phi\rangle}\right]^{1/2}. \end{aligned} \tag{35}$$

Equations (34) and (35) can be solved for the coefficients a and b; these are shown in Table XIV for each of the four simulations. Note that the coefficients have only a small Reynolds number dependence.

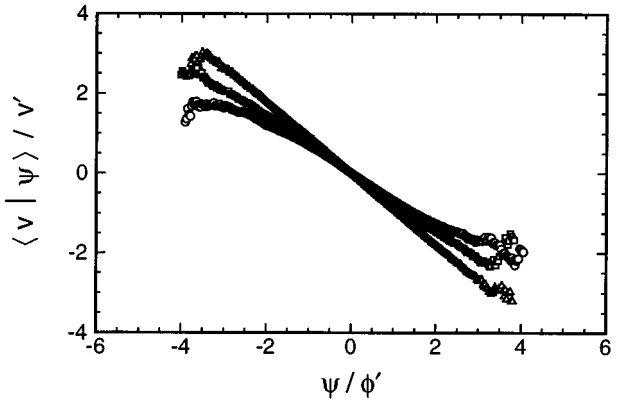

FIG. 17. Evolution of the v-velocity conditioned on the scalar. (See note in Fig. 15.) $R_\lambda = 52$: △, $0.40T_E$; □, $1.26T_E$; ○, $2.60T_E$.

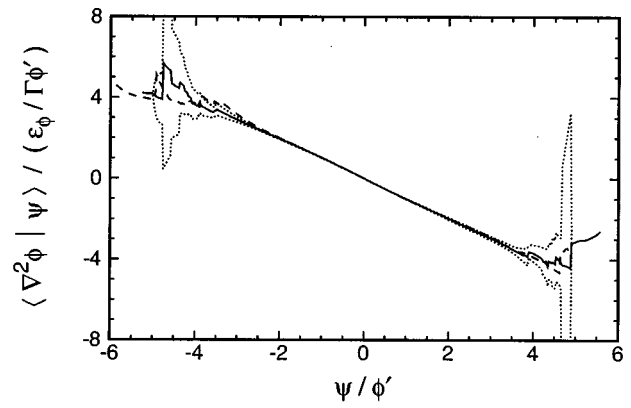

FIG. 18. Stationary expectation of the normalized $\nabla^2\phi$ conditioned on ϕ. —, $R_\lambda = 28$ (···, 90% confidence intervals); − −, $R_\lambda = 52$.

Checking the accuracy of our linear model, Eq. (32) with the above coefficients, we find slopes of 0.359 and 0.232 for Run 32.3 and Run 64.3, respectively, which is very close to the actual values. (Note: The mean of Eq. (32) conditioned on velocity is $(a\rho_{v\phi}+b)V$.) The comparison in Fig. 20 of the linear model with the jointly conditioned data is quite good in the large center region of both plots. (Recently Fox has obtained good results as well for a velocity-conditioned IEM (VCIEM) model for Eq. (31).[48])

Figure 21 shows $\nabla^2\phi$ jointly conditioned on the scalar and the scalar dissipation. In Fig. 21(a) it appears like the contours would be straight lines on a log scale. To check this Fig. 21(b) gives the results for $R_\lambda = 84$ (which are qualitatively identical to the results for $R_\lambda = 28$ in Fig. 21(a)) on a log scale, plotting only the negative half-plane of ϕ, where $\phi < 0$ and $\nabla^2\phi > 0$. However, the contours are straight (with a slope of minus 1) for only for a small region near zero.

The evolution of the expectations of scalar mixing conditioned on the scalar and v-velocity are shown in Figs. 22 and 23. The behavior does not change when conditioned on velocity; however, when conditioned on the scalar we see a slope change since the normalization uses the stationary values of scalar dissipation and rms. If each curve is normalized by its respective value of ϵ_ϕ and ϕ', then the curves are incident on each other.

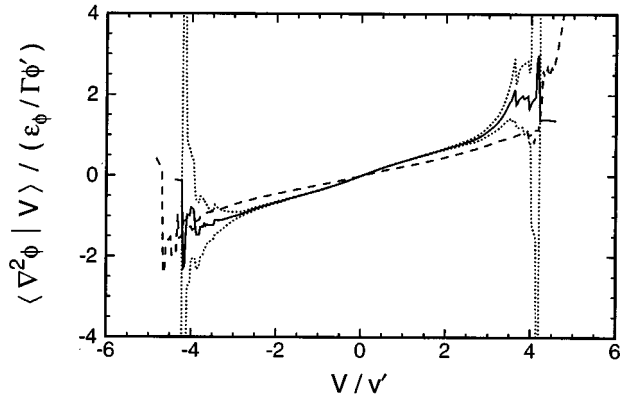

FIG. 19. Stationary expectation of the normalized $\nabla^2\phi$ conditioned on v-velocity. —, $R_\lambda = 28$ (···, 90% confidence intervals); − −, $R_\lambda = 52$.

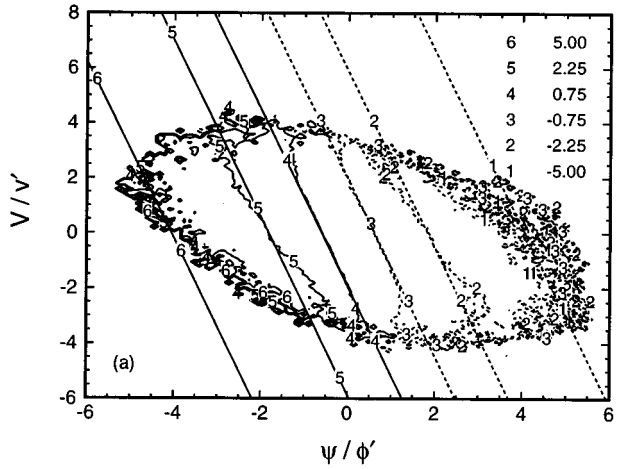

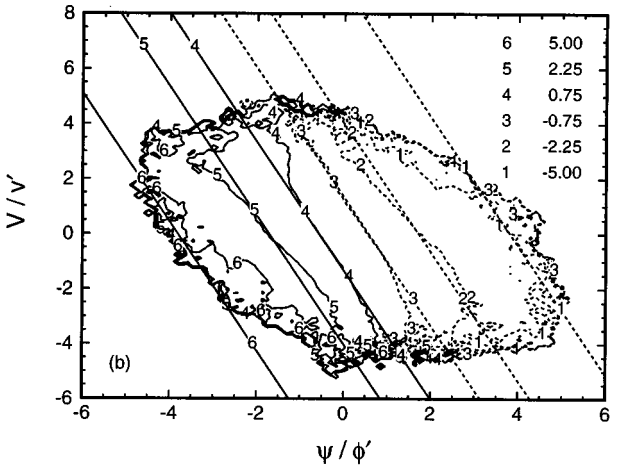

FIG. 20. Stationary expectation of the normalized $\nabla^2\phi$ jointly conditioned on ϕ and v-velocity, overlayed with contours from the linear model, Eq. (32). (a) $R_\lambda = 28$; (b) $R_\lambda = 84$.

G. Tails of the scalar pdf

We saw in the previous section that the scalar pdf is very close to a Gaussian, although its tails remain in question. Recently many have been investigating scalar pdf tails. Among these, Jayesh and Warhaft[24] found that the pdf of the scalar (temperature) fluctuations has pronounced exponential tails for values of Re_l greater than about 70, but below this critical value the pdf is close to Gaussian. The Reynolds numbers of our simulations include values both above and below this critical value.

Our first simulation is for $\mathrm{Re}_l = 46$ ($R_\lambda = 28$), so by the above hypothesis the scalar pdf should have Gaussian tails. Figure 24 shows all the scalar pdfs compared to Gaussian curves on a log scale to emphasize the tails. The result for $\mathrm{Re}_l = 46$ is also shown in a Q-Q plot in Fig. 25, where the departure of the curve from the diagonal shows the departure of the pdf from a Gaussian. (The coordinates for this Q-Q plot are (x,y), such that Prob$[\phi < x]$

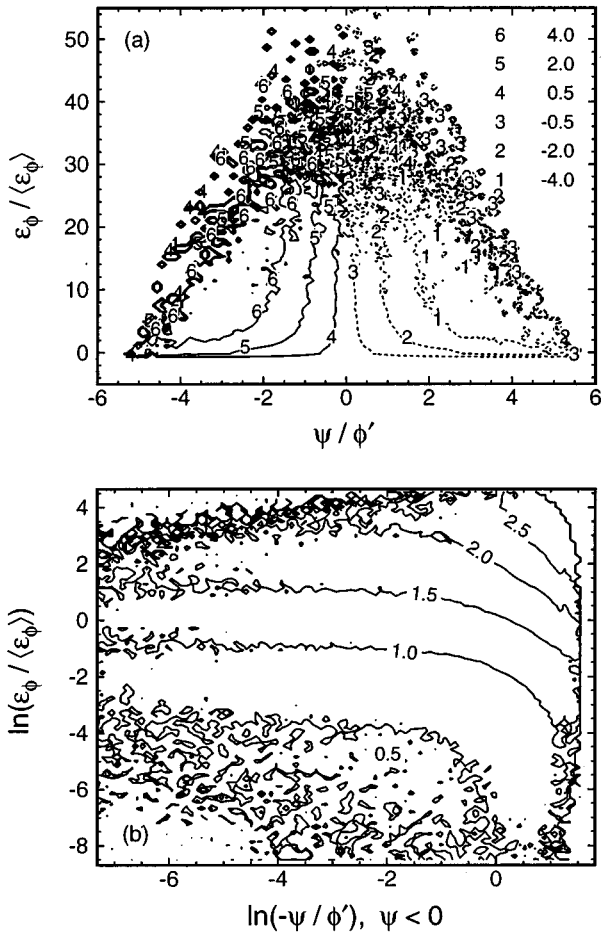

FIG. 21. Stationary expectation of the normalized $\nabla^2\phi$ jointly conditioned on ϕ and ϵ_ϕ. (a) $R_\lambda = 28$; (b) $R_\lambda = 84$. For part (b) the left half-plane where $\phi < 0$ is plotted on a log scale, with contour levels of the log of the normalized $\nabla^2\phi$.

$=$ Prob$[g<y]$, where the cumulative distribution functions for the scalar and for a Gaussian are $F_\phi(x) =$ Prob$[\phi<x]$ and $F_g(y) =$ Prob$[g<y]$.) Even though the pdf appears slightly asymmetric, it is close to the Gaussian, and the Gaussian curve is everywhere inside the confidence intervals

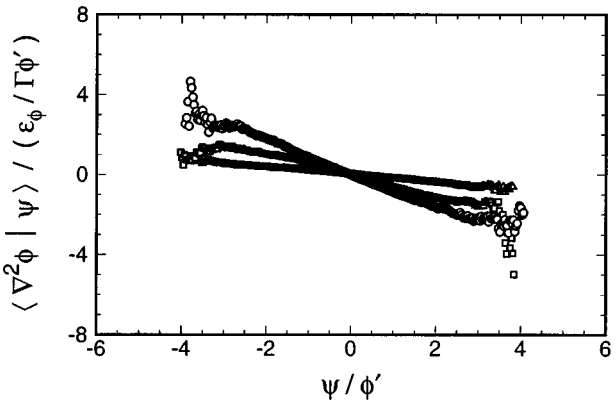

FIG. 22. Evolution of the normalized $\nabla^2\phi$ conditioned on ϕ. (See note in Fig. 15.) $R_\lambda = 52$; △, $0.40T_E$; □, $1.26T_E$; ○, $2.60T_E$.

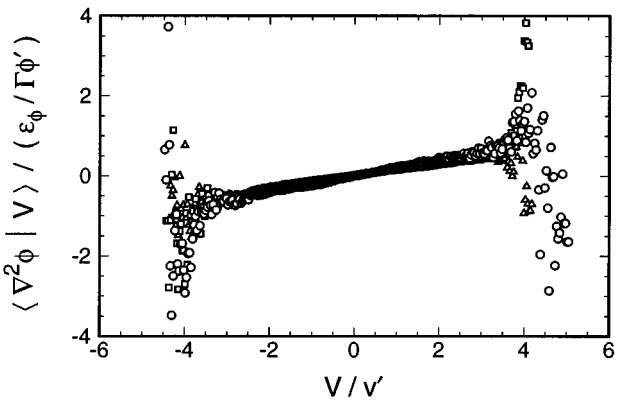

FIG. 23. Evolution of the normalized $\nabla^2\phi$ conditioned on v-velocity. (Note: Each curve is normalized by its respective instantaneous v-velocity rms value.) $R_\lambda = 52$; △, $0.40T_E$; □, $1.26T_E$; ○, $2.60T_E$.

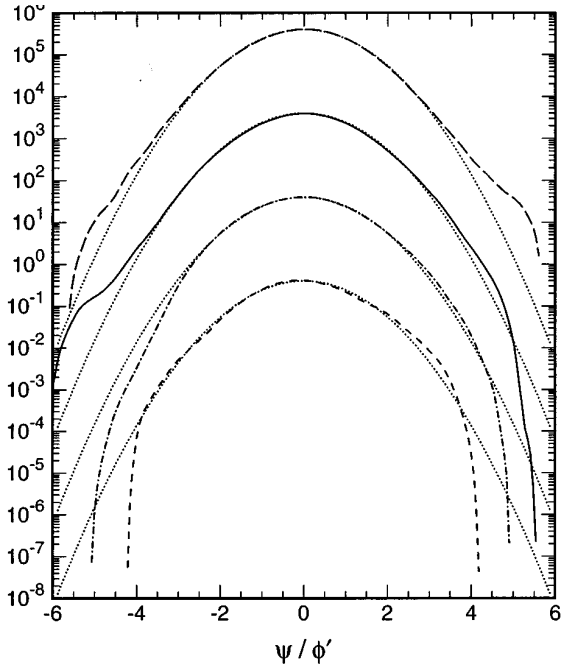

FIG. 24. Stationary standardized pdf of ϕ. Each curve has been shifted up two decades with respect to the lower one. — —, $\mathrm{Re}_l = 46$; —, $\mathrm{Re}_l = 110$; $-\cdot-$, $\mathrm{Re}_l = 243$; $--$, $\mathrm{Re}_l = 1092$; ⋯, Gaussian.

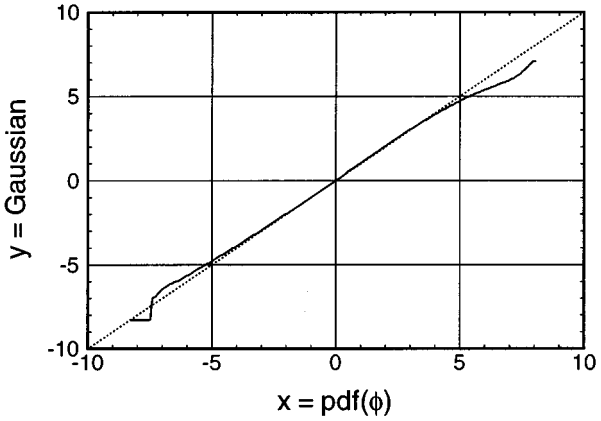

FIG. 25. Q-Q plot of the stationary standardized pdf of ϕ: y vs x for Prob$[\phi<x] =$ Prob$[g<y]$, where the g is a standardized Gaussian random variable. $\mathrm{Re}_l = 46$.

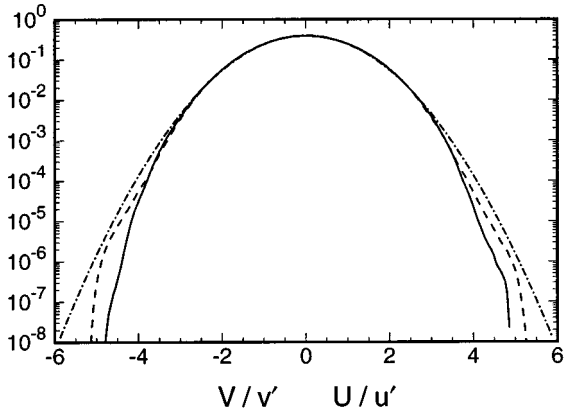

FIG. 26. Stationary standardized pdfs of v and u. $\mathrm{Re}_l = 46$. —, pdf of v; − −, pdf of u; − · −, Gaussian.

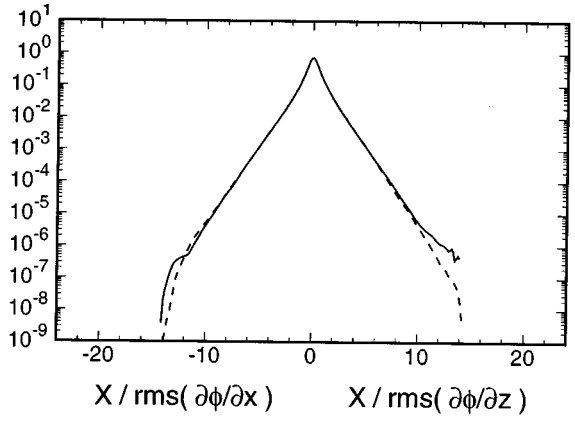

FIG. 27. Stationary standardized pdfs of $\partial\phi/\partial x$, —, and $\partial\phi/\partial z$, − −. $R_\lambda = 52$.

(not shown in the figure for clarity). Therefore, on statistical grounds one cannot say that this scalar pdf is non-Gaussian.

One observes that the center portions of the pdfs are very close to the Gaussian curves, but both (positive and negative) tails seem to droop down at their extremes. If we examine two pdfs of the turbulent velocity field (see Fig. 26) we see that they are perfectly symmetric and very close to the Gaussian one might expect them to be, but their tails also droop.

In order to investigate the effects of numerical resolution on the tails of the pdf, a simulation at this same Reynolds number was performed with twice as fine a grid, 64^3, giving a value of $k_{\max}\eta > 2$. All the results were essentially identical. Hence we can conclude that the 32^3 grid is sufficient to completely resolve this Reynolds number turbulent flow, and that a value of $k_{\max}\eta$ of 1.1 or higher, as seen in this case, gives satisfactory resolution of the pdf tails (as expected[39]).

Our 64^3 simulation is for $\mathrm{Re}_l = 110$ ($R_\lambda = 52$). From Fig. 24 it is evident that only minimal differences exist between this scalar pdf and that for $\mathrm{Re}_l = 46$; the Gaussian curve falls within the confidence intervals for both. A slight raising of the tails is echoed in the increase of the kurtosis from 2.9 for the Re_l of 46 to 3.0 here. This is the value for a Gaussian; the stretched-exponential pdfs seen in Jayesh and Warhaft[24] at similar Reynolds numbers have kurtosis values around 4.

Our 128^3 simulation is for $\mathrm{Re}_l = 243$ ($R_\lambda = 84$). The scalar pdf shown has a kurtosis of 2.9, (the same as for $\mathrm{Re}_l = 46$), and it still includes the Gaussian curve inside much of its confidence intervals. The lower value of kurtosis appears to be accounted for by the asymmetric dropping in the negative tail. This is statistical error, which is more of a problem for the two largest simulations in this study. These simulations also exhibit more pronounced drooping of the pdf tails.

The largest simulation is for $\mathrm{Re}_l = 1092$ ($R_\lambda = 185$). Here the ''stationary'' portion of the run is not very stationary on the large scale, due to large fluctuations from the forcing, only one simulation, and a short duration of slightly less than 2 eddy turnover times (see Fig. 3(d)). Hence the statistical error is high. However, the scalar pdf is still quite close to a Gaussian, with a kurtosis of 3.2.

As was seen earlier, the conditional expectations $\langle v|\phi=\psi\rangle$ and $\langle \epsilon_\phi|\phi=\psi\rangle$ confirm the overall Gaussian behavior seen here in the scalar pdfs, if allowance is made for some departure at the ends of the tails where statistical error is the highest.

These results are in contrast to the exponential pdfs found by Jayesh and Warhaft[24] for the same Reynolds numbers, but there are a number of possible reasons for this difference. It has been suggested (Tong,[49]) that this may be a result of the limited number of large eddies (integral scales) present in our DNS simulations, usually being around 5 or 6 (see Table I). They found that 8 integral scales across the tunnel width was not always sufficient to get exponential tails. It should also be remembered that the turbulence investigated by Jayesh and Warhaft[24] is decaying grid turbulence which will have different spectra than our simulations. (The Reynolds number does not fully characterize isotropic turbulence.)

However, our results are in agreement with the recent study by Jaberi *et al.*,[29] which found that the long-time scalar pdf (at $R_\lambda = 58$) is not necessarily Gaussian or exponential, but rather is sensitive to several factors. If forcing or a mean scalar gradient is present, then non-Gaussian behavior is not sustained. This study extends their result, and shows that for forced simulations with a mean scalar gradient, the scalar pdf is essentially Gaussian up to $R_\lambda = 185$.

H. Derivatives of the scalar

In contrast to the previous section, there is no shortage of experimental and DNS data for the first derivatives of the scalar, especially for $\partial\phi/\partial y$. Holzer and Siggia[18] did a number of large, high Péclet number, stationary 2-D simulations of turbulence with a passive scalar and found that the skewness in the scalar derivative persisted throughout. This skewness was also observed at low Reynolds number in the three-dimensional (3-D) DNS results of Pumir.[15]

We find a persistent skewness in $\partial\phi/\partial y$ as well. Figure 27 shows the pdfs of the scalar derivatives $\partial\phi/\partial x$ and $\partial\phi/\partial z$ for $R_\lambda = 52$, and Fig. 28 shows $\partial\phi/\partial y$ for all four simulations. The tails of these pdfs are of stretched-exponential form, and skewness is only seen in $\partial\phi/\partial y$. (Be-

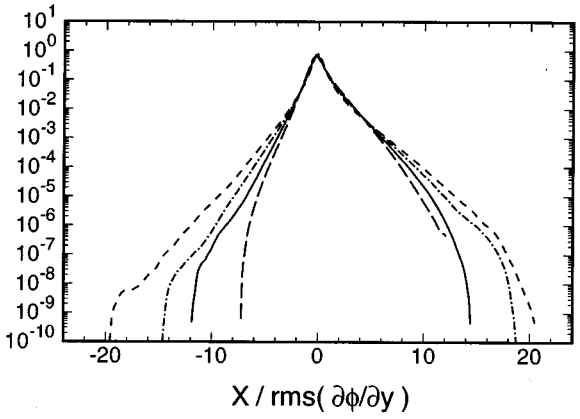

FIG. 28. Stationary standardized pdf of $\partial\phi/\partial y$. — —, $R_\lambda = 28$; —, $R_\lambda = 52$; $-\cdot-$, $R_\lambda = 84$; $--$, $R_\lambda = 185$.

cause of the symmetries in the problem, the pdfs of $\partial\phi/\partial x$ and $\partial\phi/\partial z$ are symmetric, apart from statistical variability.)

The skewness is in the positive tails; if β were negative then it would appear in the negative tails. Since the skewness is of order 1 in each case there is evidently no local isotropy of the scalar, in fact, the skewness is essentially constant with Reynolds number. Figure 29(a) shows the dependence

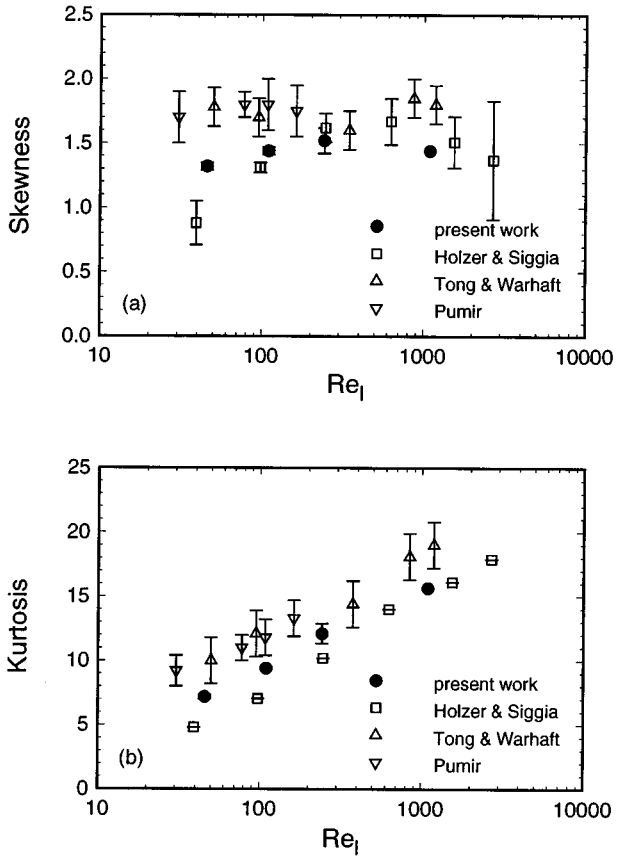

FIG. 29. Stationary moments of the pdf of $\partial\phi/\partial y$. (a) Skewness; (b) kurtosis.

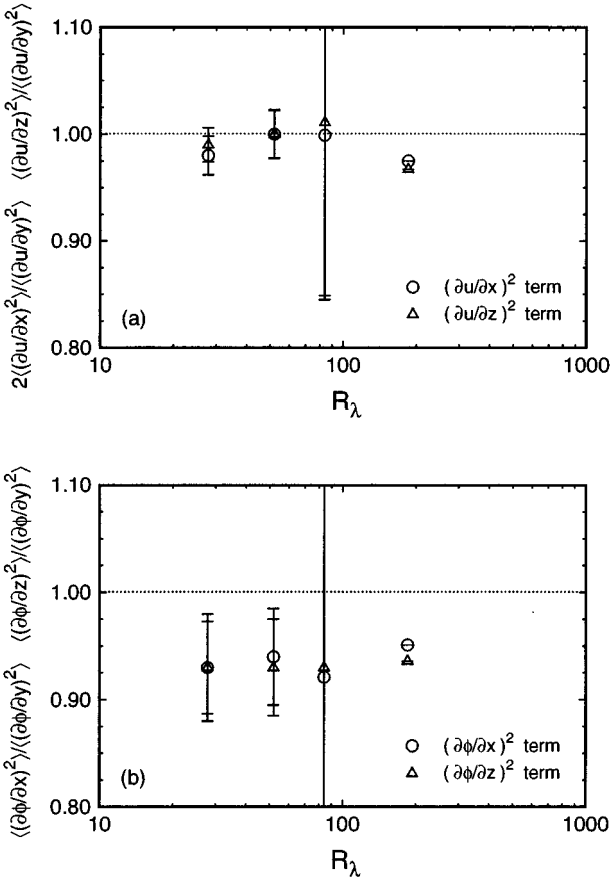

FIG. 30. Stationary mean squared gradients. The error bars indicate the 90% confidence intervals. (a) u-velocity; (b) ϕ.

of the skewness on Reynolds number, along with the results of Tong and Warhaft,[20] Holzer and Siggia,[18] and Pumir,[15] and Fig. 29(b) shows the kurtosis.

Another measure of local isotropy is the ratio of the mean squared gradients of the velocity and the scalar in different directions. In Fig. 30(a) the u-velocity field shows signs of being locally isotropic for each Reynolds number studied (up through the second-moments at least); however, that is not the case for the scalar field. In Fig. 30(b) there are small but clear differences between the scalar gradient $\partial\phi/\partial y$ and $\partial\phi/\partial x$ or $\partial\phi/\partial z$, which is due to the mean scalar gradient in the y-direction. Hence local isotropy does not hold for these scalar fields, and the situation does not change as Reynolds number increases (over the range studied).

The reason for the skewness in the scalar derivative has been shown to be the organization of the scalar in physical space. A number of researchers have observed a ramp-cliff structure in the scalar fluctuation field, which for the total scalar field (mean plus fluctuation) corresponds to cliffs separating large areas of well-mixed fluid (i.e., near constant scalar value).[21,19,18]

We find a similar structure in our results, although the effect is not pronounced. We examine a few contour plots of the scalar fluctuation here to show the orientations of the largest gradients. Figure 31 shows contours of the scalar in the constant-z plane passing through the region of maximum

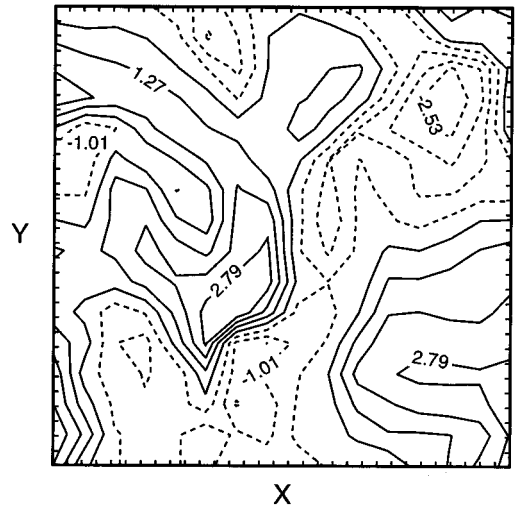

FIG. 31. Contours of the scalar through the region of highest scalar gradient magnitude. The tick marks represent the grid spacing. Contour line spacing is 0.76. $R_\lambda = 28$, $z = 24$.

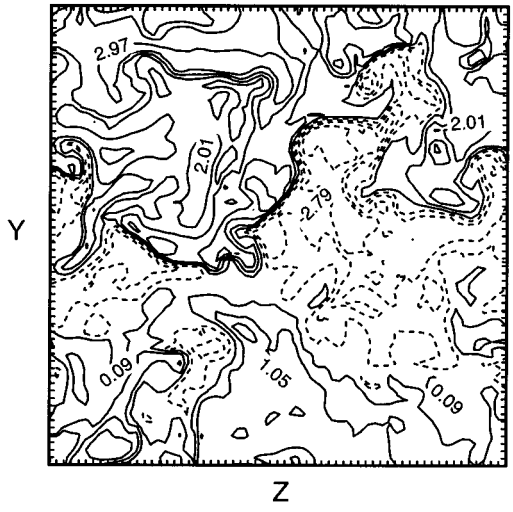

FIG. 33. Contours of the scalar through the region of highest scalar gradient magnitude. Two grid points per tick mark. Contour line spacing is 0.96. $R_\lambda = 84$, $x = 18$.

scalar gradient magnitude for $R_\lambda = 28$. Here the one cliff or steep gradient region is close to being aligned with y. (Note that the contour levels have constant spacing.) Figure 32 shows similar scalar contours for $R_\lambda = 52$. Here there are several high gradient regions, with all except one having its gradients aligned roughly parallel to y. As the Reynolds number increases the large gradient regions become more distinct. Figure 33 shows the corresponding field in a constant-x plane for $R_\lambda = 84$, and Fig. 34 for $R_\lambda = 185$. Each case shows a definite preference for the highest gradients to be parallel to y, and since these four data sets were chosen at random from the stationary portions of the four simulations (i.e., the last time step), it is likely that this effect persists throughout.

V. CONCLUSIONS

In the present study direct numerical simulations are used to investigate mixing of a passive scalar in statistically homogeneous, isotropic, and stationary turbulence, with a mean scalar gradient in the y-direction. The range of R_λ's investigated is 28 to 185. Multiple independent simulations are performed for all but the largest simulation to get confidence intervals, and local regression smoothing is used to further reduce statistical fluctuations.

After initialization of the scalar at zero, the scalar variance and scalar flux evolve to a stationary state in about 4 eddy turnover times. Contrary to former assumptions, the dissipation term in the scalar flux evolution equation is not negligible at these Reynolds numbers. Although it certainly does decrease with R_λ (as $R_\lambda^{-0.77}$), the ratio of dissipation to

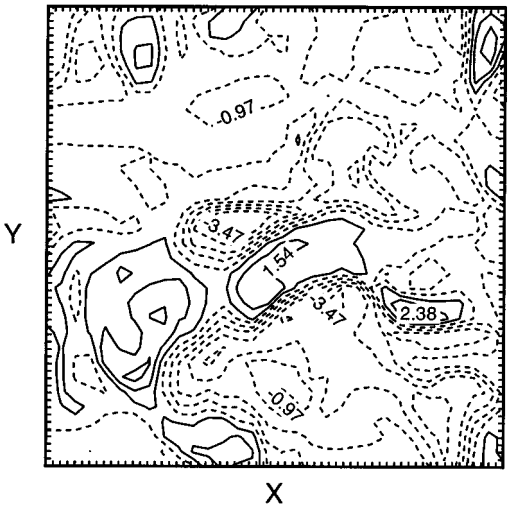

FIG. 32. Contours of the scalar through the region of highest scalar gradient magnitude. The tick marks represent the grid spacing. Contour line spacing is 0.83. $R_\lambda = 52$, $z = 52$.

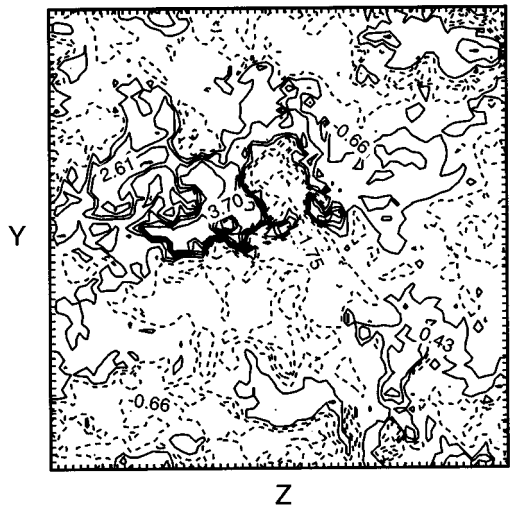

FIG. 34. Contours of the scalar through the region of highest scalar gradient magnitude. Four grid points per tick mark. Contour line spacing is 1.09. $R_\lambda = 185$, $x = 149$.

production ranges from 0.4 to 0.1 for our simulations. Extrapolating from this data, for the dissipation to be less than 5% of the production, a value of R_λ of 350 would be required. This should be checked as higher Reynolds number DNS simulations become possible.

The scalar variance and other large-scale quantities show considerable fluctuation in our simulations, due in large part to the forcing method. It would be very desirable for better forcing algorithms to be developed and employed for examining these quantities, algorithms that realistically simulate the largest scales of the energy spectrum.

Mechanical-to-thermal time scale ratios range from 1.8 to 3.0, increasing with Reynolds number. The scalar dissipation conditioned on the mechanical dissipation shows some Reynolds number dependence. It begins by increasing linearly away from a non-zero value at zero, rising to a maximum with little variability. After the maximum it becomes scattered. When conditioned on the pseudo-dissipation the maximum value is reached more quickly, and a gradual decrease towards zero at very high values of the mechanical pseudo-dissipation is evident. The pdfs of turbulent and scalar dissipation are all successfully fit to stretched exponentials, which quantitatively show the lifting of the pdf tail as Reynolds number increases.

The evolution equation for the pdf of the scalar in our study is derived and solved. From this solution two sufficient conditions arise for the scalar pdf to be Gaussian. They are: $\langle \epsilon_\phi | \psi \rangle = \langle \epsilon_\phi \rangle$ and $\langle v | \psi \rangle = -\psi/(\beta \langle \epsilon_\phi \rangle)$. We find that these conditions are well satisfied in the center of these conditional expectations (for $\psi/\phi' \in [-3,3]$); however, at the extremes $\langle \epsilon_\phi | \psi \rangle$ is not constant. It droops down towards zero, corresponding to the drooping also seen in the scalar pdf tails.

Scalar mixing, $\nabla^2 \phi$, is seen to depend on the scalar, on the log of the scalar dissipation, and on v-velocity. A linear model for scalar mixing jointly conditioned on the scalar and v-velocity is developed, and it reproduces the data quite well.

In considering the evolution of these conditional expectations, only $\langle v | \psi \rangle$ changes behavior as it evolves. Since the v-velocity variance is initially much larger than the scalar variance, the correlation $\rho(v,\phi)$ evolves from a value of unity when initialized to the stationary value of 0.5–0.6.

The tails of the scalar pdf are found to be Gaussian, or at least very nearly so, at all the Reynolds numbers examined, which is in agreement with the DNS results of Jaberi *et al.*[29] However, the grid turbulence experiments of Jayesh and Warhaft[24] at similar Reynolds numbers gave exponential tails. One possible explanation for this difference comes from Jaberi *et al.*,[29] who noted that the presence of a mean scalar gradient was sufficient to prevent the formation of exponential tails in their DNS simulations at $R_\lambda = 58$. Obviously this topic still has questions left unanswered.

We find a persistent skewness of the scalar derivative in the mean scalar gradient direction as expected, comparable to that observed by Holzer and Siggia,[18] Pumir,[15] and Tong and Warhaft.[20] An absence of local isotropy of the scalar is also evident in the mean squared gradients. No change with Reynolds number is seen.

A quick look at the organization of the scalar in physical space confirms what others have observed.[18,15] In regions of maximum scalar gradient, the steepest gradients are roughly parallel to the mean scalar gradient direction.

ACKNOWLEDGMENTS

We gratefully acknowledge support from the Department of Energy, Grant No. DE-FG02-90ER14128. Supercomputing resources were provided by the Cornell Theory Center, which receives major funding from NSF and New York State. Thanks also to our Theory Center consultant, Dr. Xianneng Shen, who often provided assistance. We also want to thank David Ruppert for the Matlab program used to smooth the pdfs, and his assistance in answering related statistics questions.

[1] S. Corrsin, ''Heat transfer in isotropic turbulence,'' J. Appl. Phys. **23**, 113 (1952).
[2] H. K. Wiskind, ''A uniform gradient turbulent transport experiment,'' J. Geophys. Res. **67**, 3033 (1962).
[3] C. C. Alexopoulos and J. F. Keffer, ''Turbulent wake in a passively stratified field,'' Phys. Fluids **14**, 216 (1971).
[4] K. S. Venkataramani and R. Chevray, ''Statistical features of heat transfer in grid-generated turbulence: Constant-gradient case,'' J. Fluid Mech. **86**, 513 (1978).
[5] Z. Warhaft and J. L. Lumley, ''An experimental study of the decay of temperature fluctuations in grid-generated turbulence,'' J. Fluid Mech. **88**, 659 (1978).
[6] A. Sirivat and Z. Warhaft, ''The effect of a passive cross-stream temperature gradient on the evolution of temperature variance and heat flux in grid turbulence,'' J. Fluid Mech. **128**, 323 (1983).
[7] P. J. Sullivan, ''Dispersion of line source in grid turbulence,'' Phys. Fluids **19**, 159 (1976).
[8] P. A. Durbin, ''A stochastic model of two-particle dispersion and concentration fluctuations in homogeneous turbulence,'' J. Fluid Mech. **100**, 279 (1980).
[9] S. Tavoularis and S. Corrsin, ''Experiments in nearly homogeneous turbulent shear flow with a uniform mean temperature gradient. Part 1,'' J. Fluid Mech. **104**, 311 (1981).
[10] S. Tavoularis and S. Corrsin, ''Experiments in nearly homogeneous turbulent shear flow with a uniform mean temperature gradient. Part 2. The fine structure,'' J. Fluid Mech. **104**, 349 (1981).
[11] R. M. Kerr, ''Higher-order derivative correlations and the alignment of small-scale structures in isotropic numerical turbulence,'' J. Fluid Mech. **153**, 31 (1985).
[12] R. M. Kerr, ''Velocity, scalar and transfer spectra in numerical turbulence,'' J. Fluid Mech. **211**, 309 (1990).
[13] G. R. Ruetsch and M. R. Maxey, ''Small-scale features of vorticity and passive scalar fields in homogeneous isotropic turbulence,'' Phys. Fluids A **3**, 1587 (1991).
[14] G. R. Ruetsch and M. R. Maxey, ''The evolution of small-scale structures in homogeneous isotropic turbulence,'' Phys. Fluids A **4**, 2747 (1992).
[15] A. Pumir, ''A numerical study of the mixing of a passive scalar in three-dimensions in the presence of a mean gradient,'' Phys. Fluids **6**, 2118 (1994).
[16] A. N. Kolmogorov, ''Local structure of turbulence in an incompressible field at very high Reynolds numbers,'' C. R. Acad. Sci. URSS **30**, 301 (1941).
[17] K. R. Sreenivasan, ''On the local isotropy of passive scalars in turbulent shear flows,'' Proc. R. Soc. London, Ser. A **434**, 165 (1991).
[18] M. Holzer and E. D. Siggia, ''Turbulent mixing of a passive scalar,'' Phys. Fluids A **6**, 1820 (1994).
[19] K. R. Sreenivasan, R. A. Antonia, and D. Britz, ''Local isotropy and large structures in a heated turbulent jet,'' J. Fluid Mech. **94**, 745 (1979).
[20] C. Tong and Z. Warhaft, ''On passive scalar derivative statistics in grid turbulence,'' Phys. Fluids **6**, 2165 (1994).
[21] D. Phong-Anant, R. A. Antonia, A. J. Chambers, and S. Rajagopalan, J. Geophys. Res. **85**, 424 (1980).
[22] A. N. Kolmogorov, ''A refinement of previous hypotheses concerning the local structure of turbulence in a viscous incompressible fluid at high Reynolds number,'' J. Fluid Mech. **13**, 82 (1962).

[23]B. Castaing *et al.*, ''Scaling of hard thermal turbulence in Rayleigh–Bénard convection,'' J. Fluid Mech. **204**, 1 (1989).
[24]Jayesh and Z. Warhaft, ''Probability distribution, conditional dissipation, and transport of passive temperature fluctuations in grid-generated turbulence,'' Phys. Fluids A **4**, 2292 (1992).
[25]A. Pumir, B. Shraiman, and E. D. Siggia, ''Exponential tails and random advection,'' Phys. Rev. Lett. **66**, 2984 (1991).
[26]A. R. Kerstein, ''Linear-eddy modelling of turbulent transport. Part 6. Microstructure of diffusive scalar mixing fields,'' J. Fluid Mech. **231**, 361 (1991).
[27]S. T. Thoroddsen and C. W. V. Atta, ''Exponential tails and skewness of density-gradient probability density functions in stably stratified turbulence,'' J. Fluid Mech. **244**, 547 (1992).
[28]V. Eswaran and S. B. Pope, ''Direct numerical simulations of the turbulent mixing of a passive scalar,'' Phys. Fluids **31**, 506 (1988).
[29]F. A. Jaberi, R. S. Miller, C. K. Madnia, and P. Givi, ''Non-Gaussian scalar statistics in homogeneous turbulence,'' in *Tenth Symposium on Turbulent Shear Flows* (The Pennsylvania State University, University Park, PA, 1995), Vol. 3.
[30]*Turbulent Reacting Flows*, 1st ed., edited by P. A. Libby and F. A. Williams (Academic Press, Great Britain, 1994).
[31]S. B. Pope, ''Computations of turbulent combustion: Progress and challenges,'' in *Proceedings of the Twenty-Third Symposium on Combustion* (The Combustion Institute, Pittsburgh, 1990), pp. 591–612.
[32]R. S. Miller, F. A. Jaberi, and P. Givi, ''Modeling and simulation of conditional scalar statistics in turbulent mixing and reaction,'' in *Tenth Symposium on Turbulent Shear Flows* (The Pennsylvania State University, University Park, PA, 1995), Vol. 2.
[33]R. O. Fox, ''The spectral relaxation model of the scalar dissipation rate in homogeneous turbulence,'' Phys. Fluids **7**, 1082 (1995).
[34]S. B. Pope, ''PDF methods for turbulent reactive flows,'' Prog. Energy Combust. Sci. **11**, 119 (1985).
[35]R. S. Rogallo, ''Numerical experiments in homogeneous turbulence,'' Technical Report No. 81315, NASA Technical Memorandum (1981).
[36]P. K. Yeung and S. B. Pope, ''Lagrangian statistics from direct numerical simulations of isotropic turbulence,'' J. Fluid Mech. **207**, 531 (1989).
[37]Y. Y. Lee and S. B. Pope, ''Nonpremixed turbulent reacting flow near extinction,'' Combust. Flame **101**, 501 (1995).
[38]P. K. Yeung and C. A. Moseley, ''A message-passing, distributed memory parallel algorithm for direct numerical simulation of turbulence with particle tracking,'' in *Proceedings of Parallel CFD '95*, edited by S. Taylor, A. Ecer, J. Periaux, and N. Satofuka (Elsevier Science Publishers, Netherlands, 1996).
[39]V. Eswaran and S. B. Pope, ''An examination of forcing in direct numerical simulations of turbulence,'' Comput. Fluids **16**, 257 (1988).
[40]D. Ruppert, private communication.
[41]T. Hastie and C. Loader, ''Local regression: Automatic kernel carpentry,'' Stat. Sci. **8**, 120 (1993).
[42]G. Comte-Bellot and S. Corrsin, ''Simple Eulerian time correlation of full- and narrow-band velocity signals in grid-generated 'isotropic' turbulence,'' J. Fluid Mech. **48**, 273 (1971).
[43]D. B. Spalding, ''Concentration fluctuations in a round turbulent free jet,'' Chem. Eng. Sci. **26**, 95 (1971).
[44]G. R. Newman, B. E. Launder, and J. L. Lumley, ''Modelling the behavior of homogeneous scalar turbulence,'' J. Fluid Mech. **111**, 217 (1981).
[45]T.-H. Shih and J. L. Lumley, ''Influence of the time scale ratio on scalar flux relaxation: Modelling Sirivat and Warhaft's homogeneous passive scalar fluctuations,'' J. Fluid Mech. **162**, 211 (1986).
[46]S. B. Pope and E. S. C. Ching, ''Stationary probability density functions: An exact result,'' Phys. Fluids A **5**, 1529 (1993).
[47]A. Sahay and E. E. O'Brien, ''Uniform mean scalar gradient in grid turbulence: Conditioned dissipation and production,'' Phys. Fluids A **5**, 1076 (1993).
[48]R. O. Fox, ''On velocity-conditioned scalar mixing in homogeneous turbulence,'' to appear in Phys. Fluids.
[49]C. Tong, private communication.